広島大学

Quark Physics Laboratory
Graduate School of Advanced Science and Engineering
Physics Program
Hiroshima University, Japan

Simulation Study to Identify Muons from Heavy Flavor Mesons in Proton-Proton and Lead-Lead Collisions at LHC ALICE Run 3

Master's Thesis

in partial fulfillment of the requirements for the degree of Master of Sciences (M.Sc)

Name: Muhamad Noor Izwan Bin Ishak
Student ID No.: M214071
Email: noor_izwan@quark.hiroshima-u.ac.jp
Supervisor: Prof. Kenta Shigaki
Chief Examiner: Prof. Kenta Shigaki
Due Date: July 25, 2023

Abstract

The primary objective of this research is to reveal the properties of the Quark Gluon Plasma (QGP) phase created during heavy ion collisions. The QGP is a state of matter that is believed to exist at extreme temperatures and densities, similar to those that existed shortly after the Big Bang. The study of the QGP provides insights into the fundamental nature of matter and the evolution of the universe.

This study focuses on investigating the properties of single heavy flavor B and D meson particles in relativistic heavy ion collisions, with a particular emphasis on their decaying process. These heavy quarks are produced through hard-scattering processes during the early stages of heavy-ion collisions and decay into muons and electrons. Heavy quarks, such as B and D mesons, offer critical insights into the properties of the Quark Gluon Plasma (QGP) phase created during heavy ion collisions. To conduct more detailed studies of QGP properties, the contribution of beauty (from B mesons) to the muon yield must be separated from that of charm (from D mesons). The measurement of charm and beauty elliptic flow will assist in gaining a comprehensive understanding of in-medium parton energy loss and thermalization. The large production yield of heavy quarks at the LHC makes the study of heavy flavor production in heavy-ion collisions of great interest. It is possible to measure both charm and beauty hadrons in similar kinematic ranges and perform a direct comparison via the "double" nuclear modification factors. Measuring the total production cross section of heavy quarks in heavy ion collisions is a crucial reference for studying the modification of quarkonia (charmonia and bottomonia) production yield, which is directly linked to the production cross section of the corresponding heavy quarks.

Muons and electrons can be detected by the forward muon spectrometer and the Muon Forward Tracker (MFT) in ALICE at LHC energies. The MFT has been incorporated into the experimental setup to improve heavy flavor measurements. The analysis includes a comparison between MFT muon simulated tracks and Monte Carlo (MC) simulations. The incorporation of the MFT into the experimental setup enables more precise measurements of heavy flavor particles, contributing to a deeper understanding of the QGP phase.

This paper focuses on the comparison of several kinematic quantities, such as the distance of closest approach (DCA), the transverse momentum (p_T), and scattering angles distributions of decay muons from B mesons, D mesons, kaons, and pions. Full simulations are conducted to study the particles produced in the forward rapidity region (-3.6 < η < -2.5) with a momentum greater than 4 GeV/c in both pp and Pb-Pb collisions. The muon tracks' shape introduces a detector bias feature that may affect the measurement results, and corrections are made after confirming the

correct algorithms for parameters. The assessment of DCA and p_T measurements is conducted for both linear and curved muon tracks to improve the separation analysis.

The results of this analysis provide critical information on the properties and evolution of the QGP, shedding light on the fundamental nature of matter under extreme conditions. Specifically, the research focuses on understanding the behavior of heavy quarks in the QGP and their decay products.

Contents

List of Figures

List of Tables

Chapter 1

Introduction

1.1 Quantum Chromodynamics(QCD)

There are currently four known fundamental interactions of nature: electromagnetic, strong, weak, and gravitational. The standard model of particle physics describes three of these interactions: strong, weak, and electroweak, all of which can involve the exchange of vector bosons. The four known vector bosons are the photon, W and Z bosons, and the gluon. They all have spin 1. The photon is responsible for the electromagnetic force, the W and Z bosons mediate the weak force, and the gluon mediates the strong force.

Quantum Chromodynamics (QCD) is a fundamental component of the standard model that describes the strong interaction between quarks and gluons, which are the particles that form hadrons including protons and neutrons. This means that, unlike the electromagnetic force, which weakens as particles separate, the strong force between hadrons becomes stronger as the distance between particles increases. This results in a phenomenon called confinement, where quarks are always confined within hadrons and cannot exist as free particles. The energy of the colour field also increases with increasing distance. At distances greater than 1 fm, it is sufficiently large to produce real quark-antiquark pairs.

In 1964, Gell-Mann and Zweig postulated that physical hadrons are composite objects made up of three quarks (baryons) or a quark-antiquark pair (mesons) [9]. These three quarks are known as the three flavors: up (u), down (d), strange (s), charm (c), bottom (b), and top (t). Gluons are the particles that mediate the strong force between quarks and come in eight different types. The eight gluons mediate the interaction between particles carrying color charge, including quarks, gluons themselves, and antiparticles. This is an important difference from the electromagnetic interaction, where the photon field quanta have no charge and cannot interact with each other. The quantum number of color can assume three values: red, blue,

and green, and antiquarks carry the anticolors anti-red, anti-blue, and anti-green. A single quark can only be detached from a hadron by producing at least two free objects carrying color: the quark and the remainder of the hadron. This implies that only colorless particles, i.e., particles with no net color, can exist as free particles, explaining why quarks are not observed as free particles.

The exchange of gluons is crucial for studying the properties of the Quark Gluon Plasma (QGP), a state of matter believed to exist at extreme temperatures and densities, similar to those shortly after the Big Bang.

Fermions	Family			Electric charge
	1	2	3	
Leptons	ν_e	ν_μ	ν_τ	0
	e	μ	τ	-1
Quarks	u	c	t	+2/3
	d	s	b	-1/3

Figure 1.1: Classification of lepton and quark types [1]

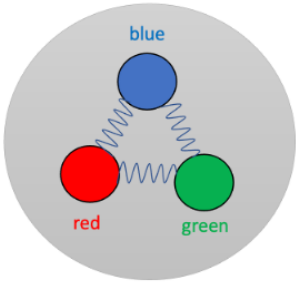

Figure 1.2: Colour quarks

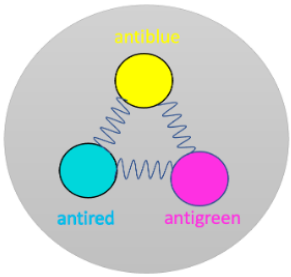

Figure 1.3: Anticolor quarks

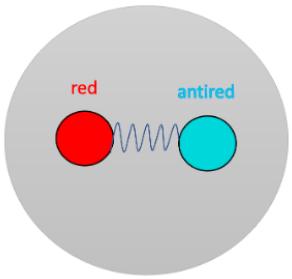

Figure 1.4: Quark-antiquark pair

1.2 Quark Gluon Plasma(QGP)

Quark-gluon plasma (QGP) is a state of matter that is believed to have existed in the early universe, just microseconds after the Big Bang. It is an exotic form of matter in which quarks and gluons, the fundamental building blocks of matter, are deconfined and behave as free particles rather than being bound within hadrons such as protons and neutrons. QGP is characterized by extremely high energy densities and temperatures, surpassing those found in ordinary nuclear matter.

The existence of this novel phase of matter was proposed in the mid-seventies, just ten years after the birth of the Quark Model of hadrons, and two years after it was realized that the candidate non-Abelian field theory of inter-quark forces predicted by QCD of their weakening at short distances, the so-called asymptotic freedom [10].

It can be said that QGP emerges as the new phase of strongly interacting matter, manifesting its physical properties in terms of nearly free dynamics of practically massless gluons and quarks. Both quarks and gluons must be present in conditions near chemical equilibrium with their color charge open for a new state of matter to be referred to as QGP.

An early discovery was that the quark-gluon plasma behaves more like a perfect fluid with small viscosity than like a gas, as many researchers had expected.

In the QGP state, the strong force, described becomes weakened, and quarks and gluons interact weakly with each other. This transition from ordinary hadronic matter to the QGP phase occurs at extreme temperatures and densities. By reaching these conditions in laboratory experiments, such as those conducted at the Relativistic Heavy Ion Collider (RHIC) at Brookhaven National Laboratory and the Large Hadron Collider (LHC) at CERN, scientists aim to study the properties and behavior of QGP [11].

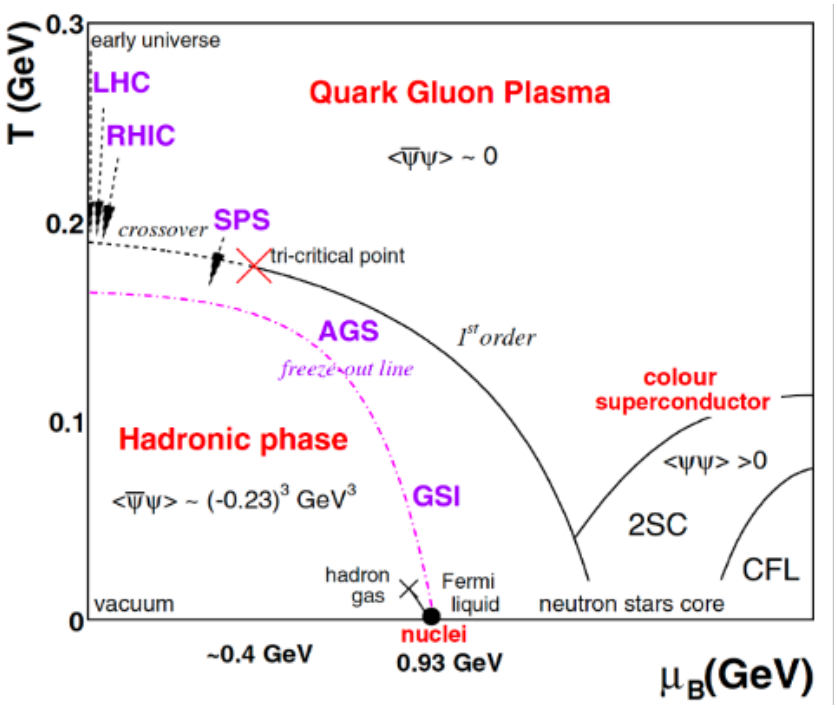

Figure 1.5: QGP state in schematic phase diagram of QCD [2]

1.3 D and B mesons in Heavy Ion Collisions

B mesons are mesons composed of a bottom antiquark and either an up quark (B^+), a down quark (B_0), a strange quark (B_0^s), or a charm quark (B_c^+). The combination of a bottom antiquark with a top quark is not thought to be possible due to the top quark's short lifetime. Similarly, a combination of a bottom antiquark with a bottom quark forms bottomonium, which is a distinct entity. These mesons are important in the study of particle physics, as they are considered as hard probes of the QGP. Researchers prefer to focus on heavy flavors (HF) since open HF states tend to be contaminated by light quarks.

The B meson has a mass of approximately 5.3 GeV/c^2, which is roughly five times the mass of a proton. It undergoes decay processes into various particles, including photons, lighter mesons, or leptons.

Beauty quark was discovered in 1977 with the discovery of upsilon meson Y($J_{PC} = 1^{--}$) as a narrow resonance at Fermi Lab and the currently measured mass is 9460.37 $\pm$ 0.21 MeV and width 52.5 $\pm$ 1.8 keV. The beauty quark is assigned quantum number B=$\pm$1. The B = -1 states ($\bar{B}^0$, B^-)$\bar{B}_s^0$ form an SU(3) triplet ($\bar{3}$) and B = -1 states (B^+,B_0)B_0^s form another triplet (3). The masses and decay time of B^- mesons (from PDG) are given below:

$B^{\pm}$ = 5279.16 $\pm$ 0.31 MeV, τ = (1.638 $\pm$ 0.11) x 10^{-12} s and

$B^{\pm}$ = 5279.53 $\pm$ 0.33 MeV, τ = (1.530 $\pm$ 0.069) x 10^{-12} s

The D meson on the other hand is a specific type of meson that consists of a charm quark and a lighter quark or antiquark. As a hadron, it is composed of quarks and gluons, specifically a charm quark and a lighter quark or antiquark. With a mass of around 1.86 GeV/c^2, the D meson is approximately twice as heavy as a proton. It can decay into different particles such as photons, lighter mesons, or leptons.

D mesons are significant as they are the lightest particles containing charm quarks. They are often studied to gain insights into weak interactions. Prior to 1986, the strange D mesons were referred to as "F mesons."

Since D mesons are the lightest mesons with a single charm quark (or antiquark), they must undergo charm (anti)quark flavor-changing transitions to decay. These transitions involve a change in the internal charm quantum number and occur solely through the weak interaction. In D mesons, the charm quark primarily transforms into a strange quark via the exchange of a W boson. Consequently, D mesons predominantly decay into kaons (K) and pions (π).

The charm quark is assigned a quantum number C = 1 and C = 0 for up, down, and strange quarks. The charge of charm quark is 2/3 and its mass $m_c = (1/2)m_{J/\psi}$ = 1.55 GeV. All charmed mesons are listed in Table ... D^+, D_0, D_s^+ ($\overline{D}_0, D^-, D_s^-$) decay weakly while $J^P = 1^-$ D-meson decay strongly and radiatively.

Charmed meson	Quark content	Mass (MeV)	Lifetime (10^{-12} sec) /Width	J^P
D^0	$c\bar{u}$	1864.54 ± 0.17	$\tau = 0.4101 \pm 0.0015$	0^-
D^+	$c\bar{d}$	1869.62 ± 0.2	$\tau = 1.040 \pm 0.007$	0^-
D_s^+	$c\bar{s}$	1968.49 ± 0.34	$\tau = 0.5 \pm 0.007$	0^-
D^{*0}	$c\bar{u}$	2006.97 ± 0.19	$\Gamma < 2.1$ MeV	1^-
D^{*+}	$c\bar{d}$	2010.27 ± 0.17	$\Gamma = (96 \pm 22)$ KeV	1^-
D_s^{*+}	$c\bar{s}$	2112.3 ± 0.7	$\Gamma \leq 1.9$ MeV	1^-
D_0^{*0}	$c\bar{u}$	2318 ± 29	$\Gamma \leq 267 \pm 40$ MeV	1^-
D_1^0	$c\bar{u}$	2422.3 ± 1.3	$\Gamma = 20.4 \pm 1.7$ MeV	1^+
D_1^+	$c\bar{d}$	–	–	1^+
D_2^{*0}	$c\bar{u}$	2461 ± 1.6	$\Gamma = 43 \pm 4$ MeV	2^+
D_2^{*+}	$c\bar{d}$	$2460.1^{+2.6}_{-3.5} \pm 1.6$	$\Gamma = 37 \pm 6$ MeV	2^+
$D_{s0}^{*\pm}$	$c\bar{s}$	2317.8 ± 0.6	$\Gamma < 3.8$ MeV	0^+
$D_{s1}^{*\pm}$	$c\bar{s}$	2459.6 ± 0.6	$\Gamma < 3.5$ MeV	1^+
$D_{s1}^{\pm}$	$c\bar{s}$	$2535.35 \pm 0.34 \pm 0.5$	$\Gamma < 2.3$ MeV	1^+
D_{s2}^*	$c\bar{s}$	2572.6 ± 0.9	$\Gamma = 20 \pm 5$ MeV	2^+

Figure 1.6: Properties of D meson types [3]

1.3.1 Importance of study of B and D mesons

The study of charm and beauty quark decays provides valuable insights into fundamental parameters of the Standard Model, such as the elements of the Cabibbo-Kobayashi-Maskawa (CKM) matrix. Furthermore, it contributes to our understanding of CP (charge-parity) violation.

There are several importances of the study of separation of charm and beauty quarks in the field of heavy ion collisions:

1. The separation between charm and beauty quarks plays a crucial role in investigating the energy loss and transport properties of heavy quarks in the QGP. When heavy quarks traverse the QGP, they experience interactions with the surrounding medium, resulting in energy loss. The energy loss mechanisms for charm and beauty quarks differ due to their distinct masses, leading to different patterns of energy degradation. By measuring the energy loss of charm and beauty quarks, scientists can extract valuable information about the QGP transport properties and gain insights into its viscosity and other relevant parameters [12].

2. Quarkonium states, such as J/ψ and Υ, which consist of a heavy quark-antiquark pair ($c\bar{c}$ and $b\bar{b}$, respectively), are sensitive to the properties of the QGP. The separation between charm and beauty quarks is crucial for understanding the suppression of quarkonium states in the QGP. The binding

and dissociation of quarkonium states are affected by the color screening and interactions with the QGP medium. The suppression patterns of charmonium and bottomonium states provide valuable information about the temperature and properties of the QGP, enabling us to explore the phase transition from a hadronic medium to the QGP [13].

3. Reconstructions of muon tracks is important to separate the beauty contribution from that of charm quarks. At the LHC, single muons are mainly produced through D hadrons, B hadrons and light hadrons. q Studies of charmed and beauty sectors in Pb-Pb collision will provide information on the fragmentation, hadronization of heavy quarks and new information on weak annihilation process [14].

4. The charm/beauty separation will enable us to investigate experimentally the mass, colour charge dependences, and energy loss of heavy quarks, light quarks and gluons Two other benefits of separation: (1) Providing important reference for the study of charmonium (or bottomonium) suppression and regeneration in QGP. (2) Comprehensive understanding of in-medium parton energy loss and thermalization [15].

5. Heavy quarks, due to their large masses, exhibit a reduced diffusion coefficient compared to light quarks in the QGP. The separation between charm and beauty quarks allows for the study of the mass dependence of heavy quark diffusion, providing insights into the interplay between the QGP medium and heavy quark dynamics [16].

6. Charm and beauty quarks have different interaction rates with the QGP due to their mass difference. Studying their thermalization processes contributes to our understanding of the dynamics of heavy quarks in the QGP medium and the time scales associated with equilibration.

1.3.2 Decay Process of D and B mesons

The decay of a D meson into a muon typically proceeds through the weak interaction mediated by the exchange of a W boson. There are several possible decay channels for a D meson into a muon, depending on the specific type of D meson involved.

One of the most common decay channels for a neutral D meson (D^0) into a muon is the so-called semileptonic decay, where the D meson decays into a muon and its associated neutrino. The specific decay process is: $D^0 \rightarrow \mu^- + \upsilon_\mu$. In this decay, the D^0 meson, which consists of a charm quark (c) and an up antiquark (u),

transforms into a muon (μ^-) and its associated neutrino (v_μ). It's important to note that the D^0 meson can also undergo flavor-changing decays, where it transforms into a strange meson (K meson) and a muon-antimuon pair. However, the semileptonic decay channel described above is the dominant one.

For charged D mesons (D^+ and D_s^+), the main decay channel into a muon involves the decay of the charm quark (c) into a strange quark (s) and the emission of a W boson. The specific decay process for a charged D meson is:

$D^+ \rightarrow \mu^+ + \nu_\mu$

$D_s^+ \rightarrow \mu^+ + v_\mu$

In these decays, the charged D meson transforms into a muon (μ^+) and its associated neutrino (v_μ) by changing the charm quark (c) into a strange quark (s) through the weak interaction.

It's important to note that there can be additional secondary decay processes occurring after the initial D meson decay, such as the subsequent decay of the produced muon. However, the main decay channel of a D meson into a muon involves the direct transformation of the charm quark into a muon, accompanied by the emission of a W boson.

The branching ratio of a specific decay channel represents the probability that a particle will decay through that channel compared to all possible decay channels. The branching ratio is typically given as a percentage or a fraction.

For the decay $D^0 \rightarrow \mu^- + v_\mu$, the branching ratio is estimated to be around 6.9%. This means that approximately 6.9% of all D^0 mesons that decay will do so through this specific channel.

For the decays $D^+ \rightarrow \mu^+ + \nu_\mu$ and $D_s^+ \rightarrow \mu^+ + v_\mu$, the branching ratios are approximately 17% and 6%, respectively. These values indicate that around 17% of all D^+ mesons and 6% of all D_s^+ mesons that decay will undergo these specific decay channels.

1.3.3 Main Decay Channel of D and B Mesons

The main decay channel of a B meson into a muon typically involves the weak interaction mediated by the exchange of a W boson. Similar to the decay of D mesons, there are several possible decay channels for a B meson into a muon, depending on the specific type of B meson involved.

One of the most common decay channels for a neutral B meson (B^0) into a muon is the semileptonic decay, where the B meson decays into a muon and its associated neutrino. The specific decay process is: $B^0 \rightarrow \mu^- + v_\mu$. In this decay, the B^0 meson, which consists of a bottom quark (b) and an up antiquark (u), transforms into a muon (μ^-) and its associated neutrino (v_μ). This semileptonic decay channel

is the dominant one for neutral B mesons.

For charged B mesons (B^+ and B_s^0), the main decay channel into a muon involves the decay of the bottom quark (b) into a charm quark (c) and the emission of a W boson. The specific decay processes for charged B mesons are:

$B^+ \rightarrow \mu^+ + v_\mu$, and $B_s^0 \rightarrow \mu^+ + v_\mu$.

In these decays, the charged B meson transforms into a muon (μ^+) and its associated neutrino (v_μ) by changing the bottom quark (b) into a charm quark (c) through the weak interaction.

It's important to note that there can be additional secondary decay processes occurring after the initial B meson decay, such as the subsequent decay of the produced muon. However, the main decay channel of a B meson into a muon involves the direct transformation of the bottom quark into a muon, accompanied by the emission of a W boson.

For the decay $B^0 \rightarrow \mu^- + v_\mu$, the branching ratio is estimated to be around 1.1%. This means that approximately 1.1% of all B^0 mesons that decay will do so through this specific channel.

For the decay $B^+ \rightarrow \mu^+ + v_\mu$, the branching ratio is estimated to be approximately 10%. This indicates that around 10% of all B^+ mesons that decay will undergo this specific decay channel.

For the decay $B_s^0 \rightarrow \mu^+ + v_\mu$, the branching ratio is estimated to be around 1.1% as well. This means that approximately 1.1% of all B_s^0 mesons that decay will undergo this specific decay channel.

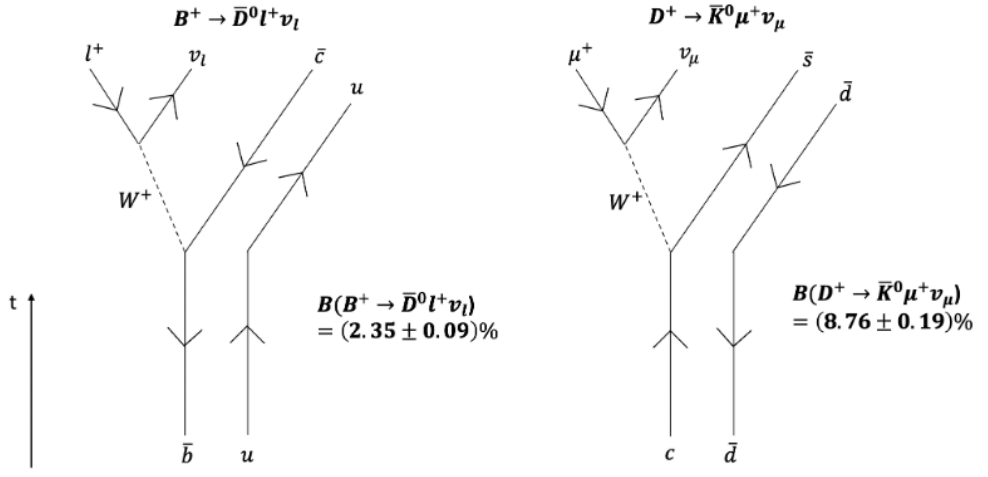

Figure 1.7: Another decay channels of B and D mesons into another mesons. Branching ratio of both decays: $B(B^+ \rightarrow \overline{D}_0 l^+ v_l)$ = 2.35 $\pm$ 0.09% and $B(D^+ \rightarrow K^+ \mu_+ v_\mu)$ = 8.76 $\pm$ 0.19% [4].

1.4 Purpose of the study

The main objective of this study is to identify decay muons originating from B mesons and D mesons in heavy-ion collisions. We measure the decay of B and D mesons into muons to extract various decay parameters, including meson decay vertices (x, y), decay angles (θ, ϕ), transverse momentum (p_T), and the distance of closest approach (DCA). To reconstruct the particles' tracks, we utilize collision simulations from PYTHIA 8 and the O2 (Online-Offline) framework.

This paper focuses primarily on the measurement of p_T and DCA, as they provide valuable information about the displacement of muons from the collision vertex (also known as the primary vertex). The distinct lifetimes of beauty and charm decays result in differences in the displacement. We anticipate that the parameters of p_T and DCA will offer clear distinctions between various types of decay muons, allowing us to distinguish between signal muons (originating from B and D mesons) and background muon sources (such as kaons, pions, and others).

Chapter 2

Simulation and Experimental Circumstances

2.1 ALICE Experiment

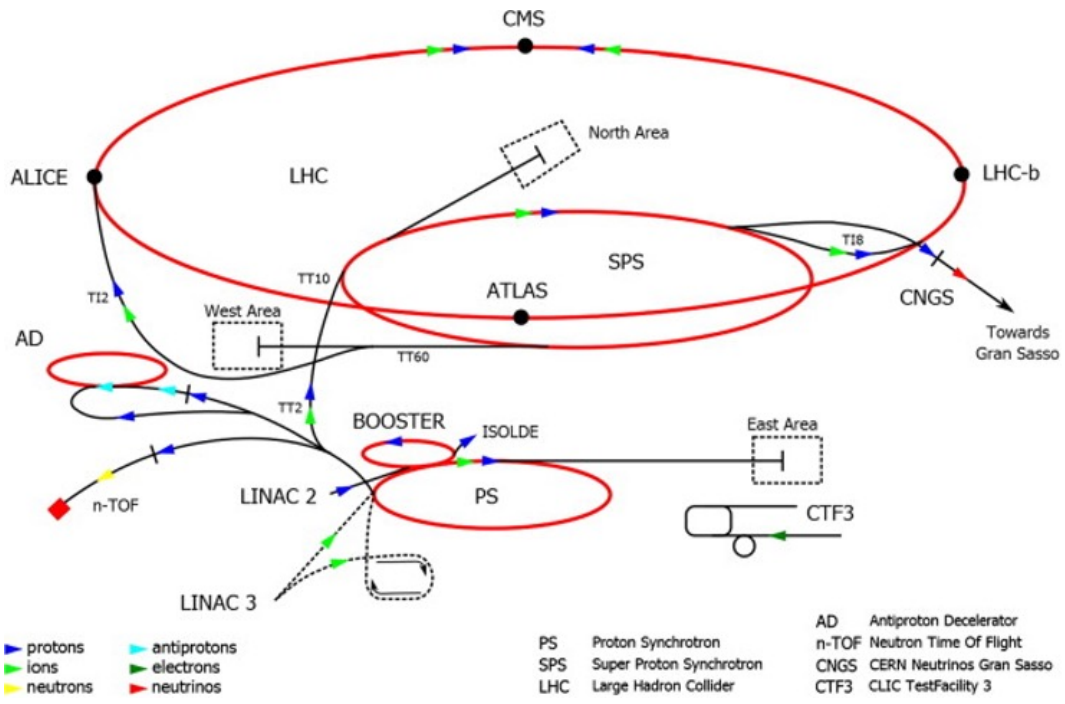

Figure 2.1: Layout of Large Hadron Collider (LHC)

The ALICE (A Large Ion Collider Experiment) is one of the major experiments conducted at the Large Hadron Collider (LHC), located at CERN (European Organization for Nuclear Research) in Geneva, Switzerland. ALICE focuses on studying the properties of matter created in ultra-high-energy heavy-ion collisions.

ALICE was specifically designed to investigate the behavior of QGP, exploring the phase transition toward the normal hadronic matter. In Run 3 the focus is on

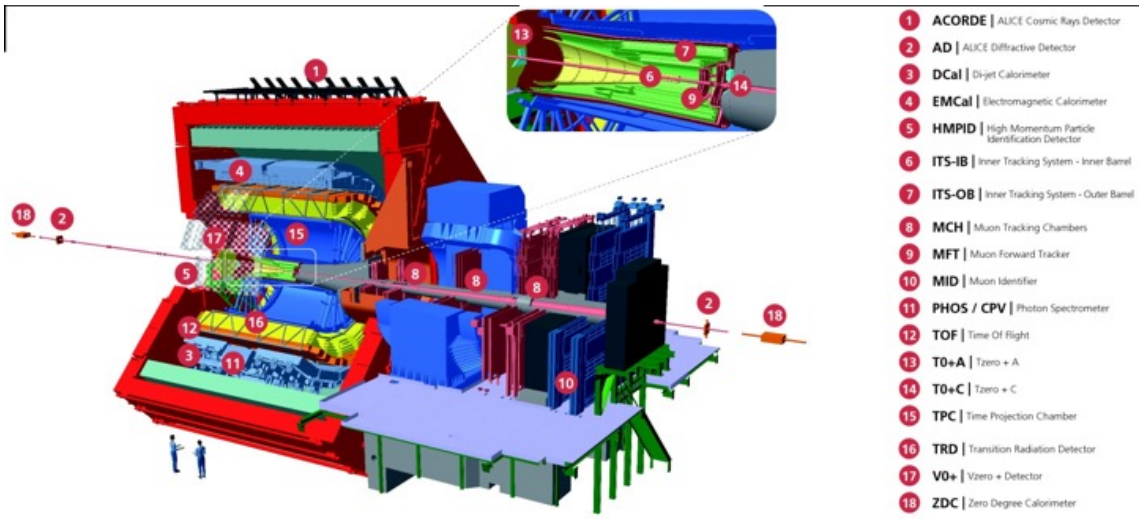

Figure 2.2: Components of ALICE Run-3 [5]

rare processes such as production of heavy-flavour particles, quarkonium states, real and virtual photons and heavy nuclear states. This grand experiment will hopefully lead to the study of the production of exotic particles and search for new physics phenomena. The ALICE detector is a complex and sophisticated apparatus designed to measure the various particles produced in heavy-ion collisions. It consists of several sub-detectors, each serving a specific purpose.

The Run 3 of the LHC, which includes the ALICE experiment, is scheduled to take place in the 2021-2024 timeframe. In Run 3, the collision energy in the beam center-of-mass system can reach $\sqrt{s_{NN}}$ = 13.6 TeV for proton-proton (pp) collisions and $\sqrt{s_{NN}}$ = 5.5 TeV per nucleon pair for Pb-Pb collisions, which are the highest collision energies in the world. ALICE detector is about 10 000-tonne– 26 m long, 16 m high, and 16 m wide. The detector sits in a vast cavern 56 m below ground close to the village of St Genis-Pouilly in France, receiving beams from the LHC.

The Run 3 of the LHC is capable of enhancing the particle measurement in low transverse momentum, p_T region and improve particle tracking capability, allowing data taking at substantially higher rates and preserving the already remarkable particle identification capabilities from Run 1/Run2.

2.2 Muon Forward Tracker (MFT)

The MFT (Muon Forward Tracker) is a high-resolution silicon-tracking detector designed to reconstruct the trajectories of muons emitted at forward angles during heavy-ion collisions. It is a silicon pixel detector positioned upstream of the

hadron absorber, with a coverage spanning -3.6 < η < -2.5 and encompassing a full azimuthal angle range.

The primary motivation behind integrating the MFT into the ALICE setup is to align the extrapolated muon tracks originating from the tracking chambers post-absorber with the clusters detected in the MFT planes pre-absorber. This alignment facilitates accurate associations between the muon tracks and MFT clusters, resulting in improved pointing accuracy of the muon tracks. Consequently, a reliable measurement of their offset relative to the primary vertex of the interaction becomes achievable.

The MFT consists of two half cones, each equipped with five half-disks positioned along the beam axis between -46 cm and -76.8 cm from the interaction point. This configuration allows for precise measurements of charged particle passages and provides valuable information regarding the distance of closest approach of the muon track to the primary vertex.

Furthermore, the MFT's capabilities are essential for c/b muon separation, enabling the distinction between charm (c) and bottom (b) muons based on their unique trajectories and interactions within the detector [17]. Such functionality contributes significantly to the accurate identification and analysis of muons emitted in heavy-ion collisions within the ALICE experiment.

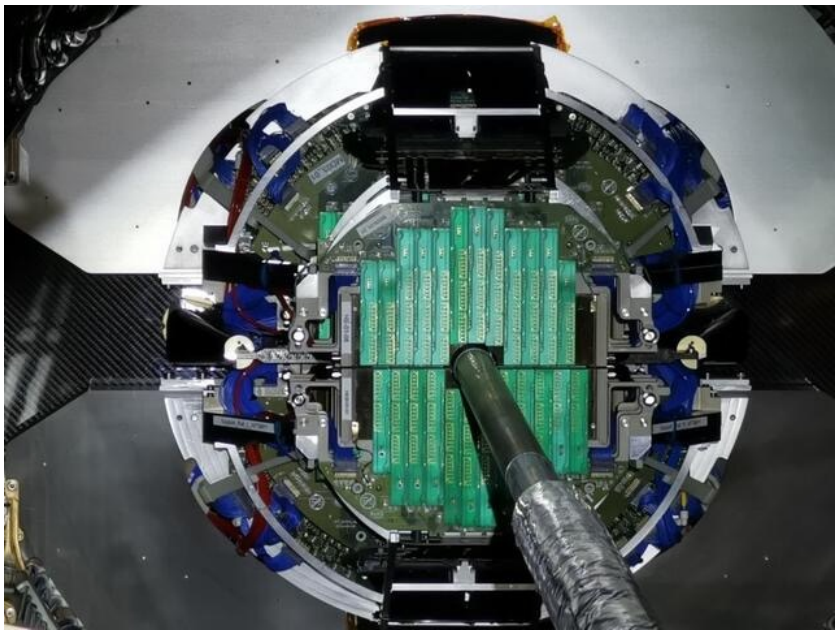

Figure 2.3: MFT half disks

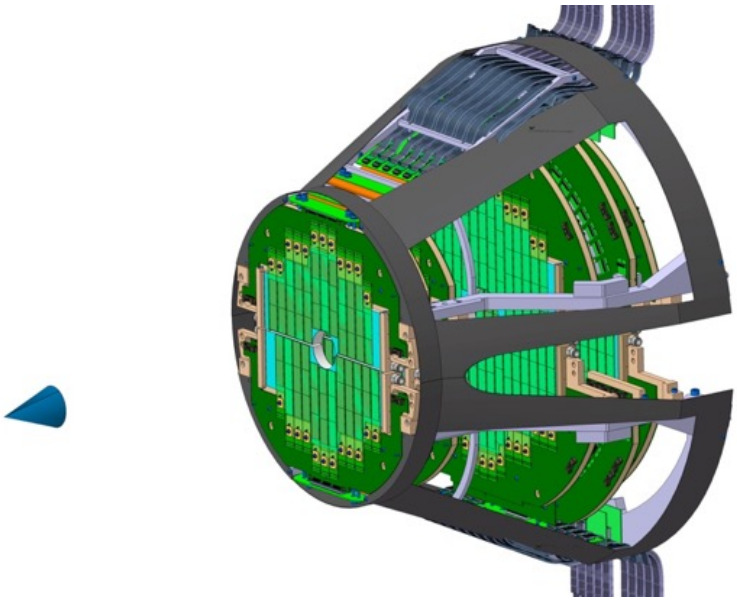

Figure 2.4: MFT Geometry

2.3 Muon Spectrometer

The Muon Spectrometer, aside from MFT is also primarily responsible for measuring the trajectories and momenta of muons produced in heavy-ion collisions. The invariant mass resolution of the muon spectrometer is of the order of 70 MeV in the J/Ψ region and about 100 MeV close to the Υ. These values allow to resolve and measure individually all five resonance states. The main components of the spectrometer are shown in Figure xx below.

Components of the muon spectrometer consists of an absorber to filter the background, a set of tracking chambers before, inside and after the magnet and a set of trigger chambers.

1. The front absorber suppresses all particles except muons coming from the interaction vertex. It is made of carbon and concrete in order to reduce the multiple scattering and muon energy loss. The inner beam shield protects the chambers from background originating from particles at small angles. It is made of tungsten, lead and stainless steel to reduce the background arising from primary particles emitted in the collision and from their showers produced in the beam pipe and in the shield itself.

2. The tracking system is made of 10 cathode pad/strip chambers arranged in 5 stations of 2 chambers each. The spatial resolution should be better than 100 mm and all the chambers are made of composite material to reduce the scattering of the muons in order to obtain the required resolution. To limit the

occupation rate to a maximum of 5% the full set of chambers has more than 1 million channels.

3. The trigger system is designed to extract heavy quark resonance decays. The selection is made on the p_T of the two individual muons. The 4 planes of RPCs (Resistive Plate Chambers) arranged in 2 stations and put behind a passive muon filter to measure the transverse momentum of each muon.

4. The dipole magnet is positioned at about 7 m from the interaction vertex and it is one of the biggest warm dipoles in the world (free gap between poles ≈ 3 m, height of the yoke ≈ 9 m). The magnetic field (B_{nom} = 0.7 T, 3 Tm field integral) is defined by the requirements on the mass resolution.

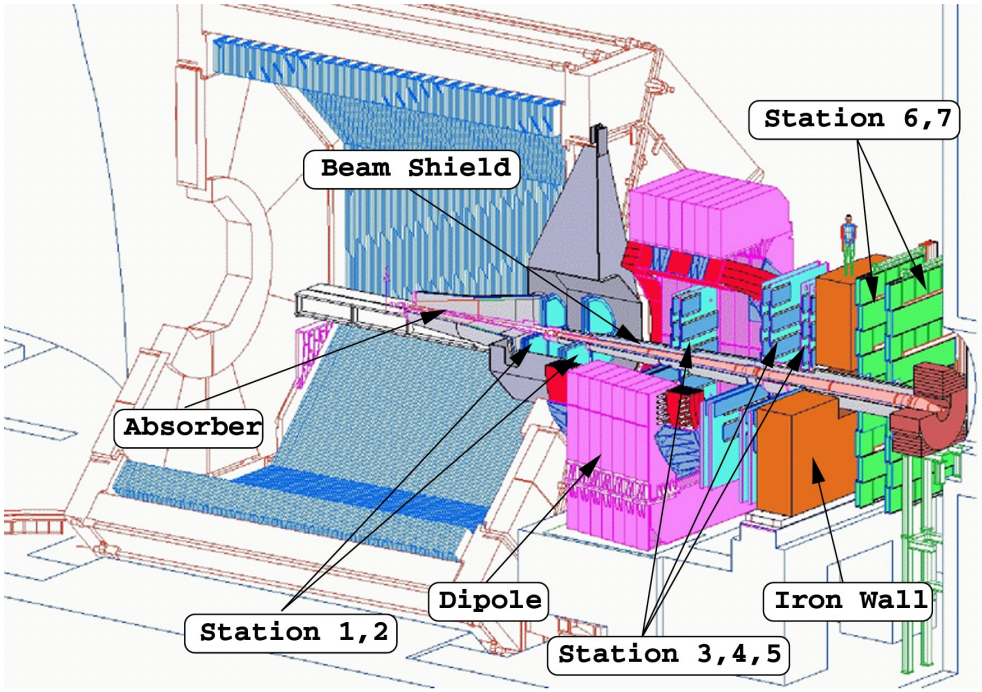

Figure 2.5: Layout of the muon spectrometer. The tracking system consists of stations 1 to 5 and trigger system of stations 6 and 7 [6]

2.4 O2 (Online-Offline) Data Framework

The O2 (Online Offline) data processing framework is a critical component of the ALICE (A Large Ion Collider Experiment) project at CERN (European Organization for Nuclear Research). It serves a dual purpose, providing a unified framework for both online data processing during data acquisition and offline data analysis to extract meaningful physics results.

Built on top of the widely-used ROOT data analysis framework, O2 leverages ROOT's rich set of tools and libraries while extending them to meet ALICE's specific requirements. Its modular and scalable design enables distributed and parallel processing across multiple computing nodes, following a component-based architecture that accommodates evolving experiment needs.

A key feature of O2 is its ability to perform real-time online data processing. As raw detector data is continuously streamed, O2 processes and reconstructs it on-the-fly, offering immediate feedback and monitoring for informed decision-making during data acquisition.

Online data processing in O2 involves stages such as data decoding, calibration, reconstruction, and event building. Raw data is decoded to extract information, then calibrated to correct for electronic noise and detector response. Event reconstruction identifies and measures individual particles and their properties. Finally, the reconstructed events are organized into larger structures for further analysis.

O2 provides a high-level interface and APIs for efficient data analysis, offering tools and libraries for event reconstruction, particle identification, track finding, and data visualization. It also incorporates advanced data management capabilities, utilizing distributed file systems and data caching to ensure efficient storage and retrieval of large-scale datasets.

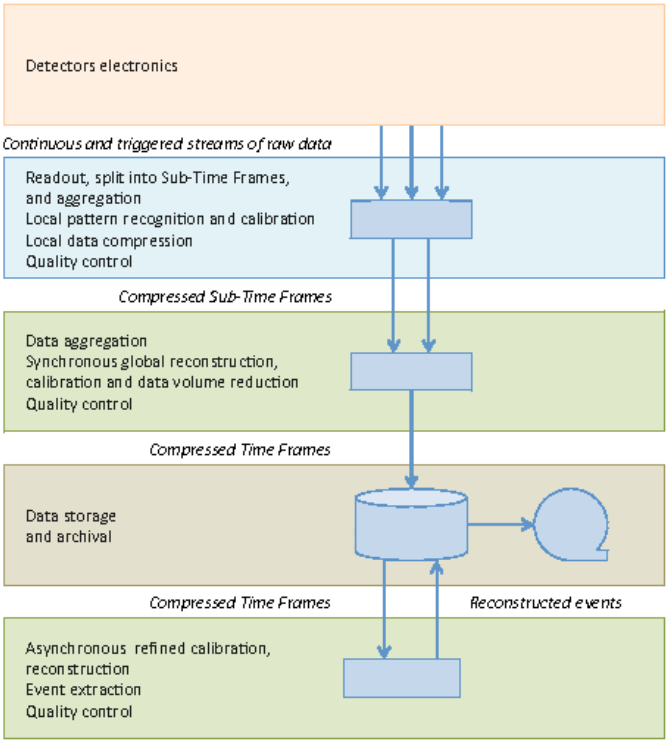

Figure 2.6: Data volume reduction in O2 framework [7].

Performance is optimized through modern computing technologies like multi-threading and GPU acceleration, allowing timely analysis and quick feedback during the experiment.

The ALICE Computing Model for Runs 3 and 4 aims to reduce data volume as early as possible during data-flow. Zero-suppressed data from all collisions will be shipped to the O2 facility. Data volume reduction will be achieved through synchronous reconstruction steps during data taking, storing data temporarily at high speeds.

The O2 facility will be a high-throughput system, utilizing heterogeneous computing platforms with hardware acceleration. The O2 software framework will provide abstraction for common code to function on different platforms, supporting concurrent computing models across various facilities. Open-source software conforming to open standards will be used whenever possible, enhancing flexibility and adaptability.

2.5 Geant4

Geant4 is a toolkit used for the simulation of the passage of particles through matter, including the interactions of particles with matter. It is used extensively in high-energy physics experiments, including those at the LHC, and is also used in other fields such as medical physics and nuclear engineering.

In the context of O2, Geant4 is used to simulate the interactions of particles with the detector material in both pp and Pb-Pb collisions. The simulation of pp collisions using Geant4 involves simulating the passage of particles through the various layers of the detector, including the inner tracking detectors, the calorimeters, and the muon chambers. The simulation takes into account the effects of particle interactions with the detector material, including energy loss due to ionization and radiation, as well as multiple scattering and particle decays.

To simulate complex process like p-Pb and Pb-Pb, Geant4 is also used in conjunction with other simulation tools such as the HIJING event generator and the UrQMD hadronic transport model to simulate the evolution of the collision from its initial stage to the final hadronic state. The simulation takes into account the effects of particle interactions with the dense nuclear matter created in the collision, as well as the propagation of particles through the detector material.

In both pp and Pb-Pb collisions, the output of the Geant4 simulation is a set of simulated detector hits, which can be processed in the same way as the real detector data. This allows for a direct comparison of the simulated and measured observables, and allows for the estimation of the detector acceptance, efficiency, and resolution.

Furthermore, Geant4 also supports multiple visualization frameworks, including Open Inventor, OpenGL, and HepRep [18]. These frameworks allow for the creation of 3D visual representations of the detector geometry and the simulated particle tracks.

2.6 Pythia 8

Pythia 8 is an important Monte Carlo event generator utilized extensively in ALICE experiment for both the simulation of collision events and the generation of background events for data analysis. The program contains theory and models for a number of physics aspects, including total and partial cross-sections, hard and soft interactions, parton distributions, parton showers for initial and final states, merging and matching of matrix elements and showers, interactions involving multiple partons, hadronization/fragmentation, and decays. It is largely based on original research but also incorporates numerous formulae and other knowledge from the literature. The code package includes interfaces for input from and output to other programs, but the core can function independently, and it encompasses sufficient tools to facilitate straightforward analyses. It also has a set of utilities and interfaces to external programs. Unlike previous version of the program, Pythia 8 is written in programming language of C++.

Strengths of Pythia 8 lie in specialized physics models, detailed parton showers, and hadronization simulations. However, it does not simulate the detector response, and its event-by-event fluctuations might introduce limitations in precision studies. So, Pythia 8 is used in conjunction with other simulation and reconstruction software (such as JETSET) to simulate the entire data acquisition and analysis process. The simulated events generated by Pythia 8 serve as input to the ALICE detector simulation, where they are propagated through the detector elements to simulate the particle interactions and response of the detector. This step accounts for the detector resolution, efficiencies, and other instrumental effects, allowing for a realistic reconstruction of the measured data.

Over the last 40+ years, PYTHIA/JETSET has seen extensive use at almost all high-energy colliders. These colliders include PETRA, PEP, TRISTAN, SLC, and LEP for e^+e^- collisions, HERA for ep collisions, Tevatron for $p\bar{p}$ collisions, and LHC for pp/pA/AA collisions. PYTHIA/JETSET has also played a significant role in the study of proposed future colliders, fixed-target experiments, and cosmic-ray investigations, among others. Its versatility extends across all project stages, from initial feasibility studies to detector design, search/analysis strategy development, and data interpretation [19].

2.7 Track Matching

In the context of B and D meson decays, the primary goal is to match muon tracks from these decays with their corresponding tracks in the ITS, TPC, and Muon Spectrometer. This crucial process allows for the accurate determination of the muon's momentum, decay vertex position, and other essential parameters.

Track matching in the ALICE detector involves several essential methods to identify and associate tracks from the same particle. Pattern recognition algorithms analyze detector responses, leveraging spatial information from ITS, TPC, and the Muon Spectrometer to identify common patterns and extrapolate tracks. Statistical techniques consider measurement uncertainties to determine track associations' likelihood, effectively minimizing misidentifications and false matches.

Ensuring reliable matched tracks, quality criteria evaluate parameters like track fit chi-square, hit count, and overall compatibility with measured data. Particle identification techniques play a crucial role in identifying muons, which is vital for studying B and D meson decays. The Muon Spectrometer's specific measurements enable the distinction of muons from other particles based on energy deposition and timing information.

Addressing the challenge of background and overlapping tracks is critical to avoid interference with desired track identification. Algorithms are employed to mitigate these effects, incorporating energy loss measurements and track quality criteria tailored for muons.

Multiple scattering and energy loss in detector materials present further challenges to track matching accuracy. To overcome these effects, corrections and calibration techniques are applied, ultimately enhancing the precision of track reconstruction.

In addition to traditional methods, advanced machine learning techniques are harnessed in the ALICE detector for track matching. Algorithms are trained on large datasets to learn correlations between detector responses and track parameters, leading to improved efficiency and reduced misidentification rates.

The combination of these methods ensures accurate track associations, enabling precise reconstruction of particle trajectories and supporting crucial studies in heavy-ion collisions within the ALICE experiment.

In LHC Run 3, the O2 framework takes center stage for simulations and analysis, with a specific focus on the decay of heavy flavor hadrons like B and D mesons into muons ($B, D \rightarrow \mu X$). Performance studies rely on HIJING for simulating background events, mainly composed of π, K particles, with signals from a PYTHIA parametrization embedded within HIJING events. To provide an accurate representation of the experimental setup, the GEANT 4 detector simulation software is

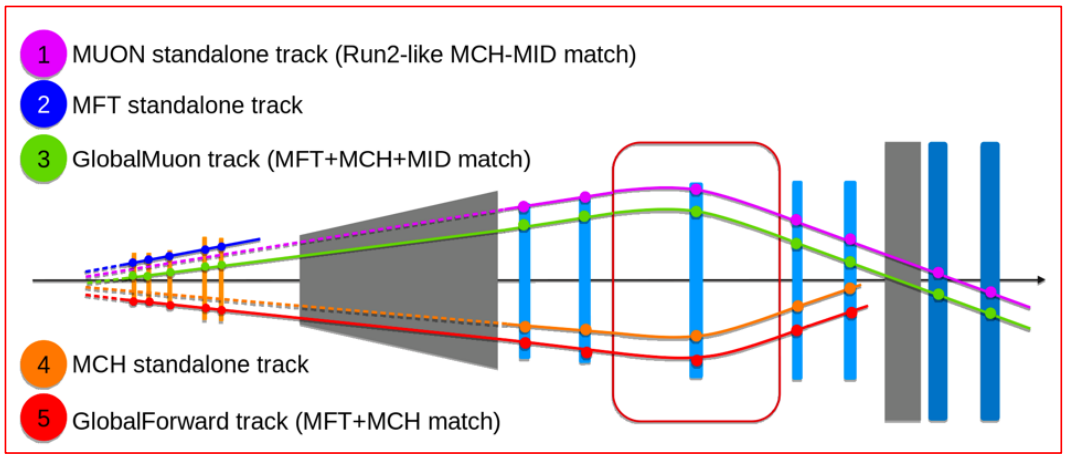

Figure 2.7: Track reconstruction in the Muon spectrometer and MFT

employed to simulate the interaction of generated particles with the ALICE detector. These tools play crucial roles in advancing our understanding of heavy flavor decays and other phenomena in heavy-ion collisions within the ALICE experiment.

2.8 Global Forward Track

The global forward track reconstruction focuses on reconstruction of the tracks of particles emitted in the forward direction, specifically in the pseudorapidity, η range of the Muon Spectrometer (MCH and MTR) in ALICE. This region is of particular interest for studying B and D meson decays because it allows for the identification and measurement of muons, which are key signatures of these decays.

The first step in the global forward track reconstruction is pattern recognition. The signals produced by the detector subsystems are analyzed to identify track segments corresponding to charged particles. In the case of muons, the MFT and Muon Spectrometer is the primary subsystem used for their detection. The muons traverse the various layers of the Muon Spectrometer, leaving energy deposits and triggering the detector readout. The pattern recognition algorithms in the Muon Spectrometer identify these energy deposits and reconstruct track segments by connecting the hits in different detector layers. The reconstructed track segments are then used as a starting point for the subsequent track fitting process.

The next step is track fitting, where the reconstructed track segments are combined and fitted to determine the full trajectory of the muon track. The track fitting algorithms use the information from the MFT and Muon Spectrometer layers to estimate the muon's momentum, direction, and position at the primary vertex. The fitted tracks are then used for further analysis and particle identification. In the case

of muons, particle identification is accomplished by exploiting the specific characteristics of muons compared to other particles. The Muon Spectrometer subsystems, MCH and MTR, provide measurements optimized for muon detection. By applying selection criteria based on energy deposition patterns, timing, and other relevant parameters, the identification algorithms can effectively identify muon tracks and distinguish them from other particles [20].

Quality selection criteria then are applied including parameters such as the number of hits in the MFT and Muon Spectrometer layers, the χ^2 of the track fit, and the track's compatibility with the measured data. These criteria help filtering out poorly reconstructed or misidentified tracks, improving the purity and quality of the final track sample.

2.9 Monte Carlo (MC) track

MC tracks used in O2 for pp collisions are typically generated using the Pythia event generator, which simulates the hard scattering of partons (quarks and gluons) in the colliding protons, as well as the subsequent hadronization and fragmentation processes. The resulting particles are then propagated through the detector geometry using a Geant4-based simulation, which takes into account the effects of particle interactions with the detector material, as well as detector response and resolution.

For Pb-Pb collisions, the MC tracks are generated using a hybrid approach that combines the HIJING event generator with the UrQMD hadronic transport model [21]. The HIJING generator simulates the initial hard scattering and parton-parton interactions in the colliding nuclei, while the UrQMD model simulates the subsequent evolution of the system, including hadronization, resonance decays, and final-state interactions. The resulting particles are then propagated through the detector geometry using the same Geant4-based simulation as in the pp case.

In both cases, the MC tracks are used to provide a simulated baseline for comparison with the real data. The MC tracks are subjected to the same reconstruction and analysis procedures as the real data, allowing for a direct comparison of the measured and simulated observables. The MC tracks are also used to estimate the detector acceptance, efficiency, and resolution, which are needed to correct the measured data for detector effects.

In addition to the standard MC tracks, O2 also employs a technique known as embedding, which allows for the simulation of specific physics processes within the context of real data events. In embedding, simulated particles are overlaid onto real data events, allowing for the study of specific physics processes such as jet quenching or heavy-ion jet tomography. The embedded particles are generated using the same Pythia or hybrid HIJING-UrQMD generators as in the standard MC tracks,

and are embedded into the real data events at the level of raw detector signals. The resulting embedded events are then subjected to the same reconstruction and analysis procedures as the real data, allowing for a direct comparison of the embedded physics process with the real data.

2.10 Transverse momentum (p_T)

The transverse momentum of a particle is the component of its momentum perpendicular to the beam axis, and it is a measure of the particle's motion in the plane perpendicular to the beam. In the study of heavy mesons such as B mesons and D mesons, the measurement of the transverse momentum distribution provides valuable information on the production mechanism and properties of these particles.

The transverse momentum distribution of B mesons and D mesons reflects the details of the production mechanism. In particular, the transverse momentum distribution can provide information on the momentum transfer between the colliding particles, which is related to the parton distribution functions (PDFs) of the colliding particles. The PDFs describe the distribution of momentum and energy carried by the partons (quarks and gluons) inside the colliding particles, and they are important inputs for theoretical calculations of particle production in high-energy collisions.

In addition to providing information on the production mechanism, the transverse momentum distribution of B mesons and D mesons is also important for the measurement of their properties. The transverse momentum affects the decay of the heavy mesons and the distribution of the decay products. For example, the transverse momentum of the B meson affects the opening angle between the two decay products in the decay B $\rightarrow$ J/Ψ + K, which is used to measure the B meson lifetime. The transverse momentum of the D meson affects the distribution of the decay products in the decay D $\rightarrow$ K$\pi\pi$, which is used to measure the D meson decay constants and form factors.

The transverse momentum of B mesons and D mesons can be measured using various techniques, depending on the experimental setup. One common method is to measure the curvature of the particle trajectory in a magnetic field. The transverse momentum is related to the curvature by the equation $p_T = qB\rho$, where p_T is the transverse momentum, q is the charge of the particle, B is the magnetic field strength, and ρ is the radius of curvature. Another method is to measure the distribution of the decay products in the laboratory frame, and extract the transverse momentum from the momentum conservation equation.

2.11 Distance of Closest Approach (DCA_T)

The Distance of Closest Approach (DCA_T) refers to the minimum distance between the trajectory of a charged particle and the primary vertex of the collision. The quantity provides necessary information about the production, propagation, and decay processes near the primary vertices. A muon track with a small DCA_T indicates a close proximity to the primary vertex and a higher probability of originating from a B or D meson decay. By measuring the displacement between the primary vertex and the point of closest approach of the track, the decay length can also be estimated. In this research, we measure the DCA_T distribution of some particles and decide certain ranges suitable for maximizing the muon signals extraction and rejecting most of background muons from other sources.

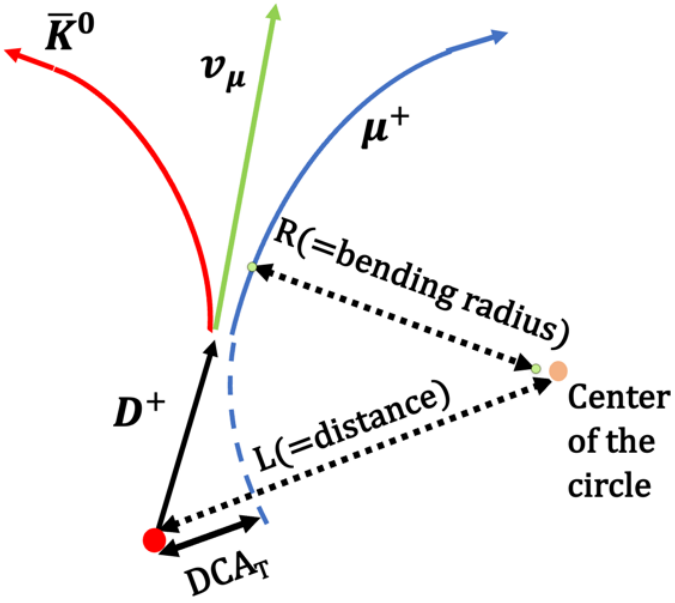

Figure 2.8: Distance of Closest Approach (DCA), the distance between a beam center and a center of the circle [8].

2.11.1 DCA calculation with cartesian coordinate

If the exact position of the muon is not given, but we have information about the decay point, muon momentum, muon momentum angles (horizontal and vertical angles), and primary vertex position, then we calculate the transverse distance of closest approach (DCA) in the following way:

1. Convert the muon momentum and angles to momentum components: $p_x = p * sin(\theta) * cos(\phi)$, $p_y = p * sin(\theta) * sin(\phi)$, and $p_z = p * cos(\theta)$ where p

is the magnitude of the muon momentum, theta is the vertical angle, and ϕ is the horizontal angle.

2. Calculate the direction vector of the muon in the transverse plane: $v_x = p_x/p$, $v_y = p_y/p$, and $v_z = 0$.

3. Calculate the vector from the primary vertex to the decay point: $d_x = decay_x - vertex_x$, $d_y = decay_y - vertex_y$, $d_z = decay_z - vertex_z$.

4. Calculate the transverse momentum of the muon in the transverse plane: $p_T = \sqrt{(p_x^2 + p_y^2)}$. Calculate the transverse displacement vector from the primary vertex to the track at a given radius r: $r = p_T/(0.3 * B)$ where B is the magnetic field strength in Tesla.

5. Calculate the transverse distance of closest approach (DCA) in the transverse plane: $DCA_X = d_x - r * v_x$, $DCA_Y = d_y - r * v_y$, and $DCA_T = \sqrt{(DCA_X^2 + DCA_Y^2)}$.

In these calculations, the muon position is not explicitly needed. Instead, muon momentum, momentum angles, and primary vertex position are utilized to determine the DCA in the transverse plane.

Chapter 3

Data Analysis – Extraction of Heavy Flavour Decay Muons

The simulation data used in this research are the pp collisions at center of mass energy $\sqrt{s_{NN}} = 14$ TeV and Pb-Pb collisions at center of mass energy, $\sqrt{s_{NN}} = 5.52$ TeV taken by ALICE Run 3 detectors. There is no minimum bias event and high multiplicity events (HM) were selected as collision types for both pp and Pb-Pb collisions. There is no centrality specified for Pb-Pb collisions. We assume that pp and Pb-Pb beams are directed at the primary vertex located at center of ITS designated as (x, y, z) = (0,0,0) cm so that collisions occur at that point. But from the Figure 3.1, the primary vertices seem to form a sharp peak pattern below 0.05 cm and are not fixed at (0,0,0) so the distance of closest approach calculation (DCA) has to take this factor into account. The number of events in pp and p-Pb collisions and parameters used in the simulations are summarized in the Table 3.1. Global muon track and Monte Carlo tracks cover the MFT forward rapidity region (3.6 < η < 2.5), with muon momentum p > 4 GeV/c, and a magnetic field is applied in the z-axis direction parallel to colliding particle beams. To identify the muons track from B and D mesons decay, it is important to reconstruct the parameters (x, y, η, θ) of each detected muons so DCA of each decay point can be calculated.

Table 3.1: Simulation Set Up for pp and Pb-Pb collisions

	$\sqrt{s_{NN}}$ [GeV]	Number of Events
pp	14	930,000
Pb-Pb	5.52	7,200

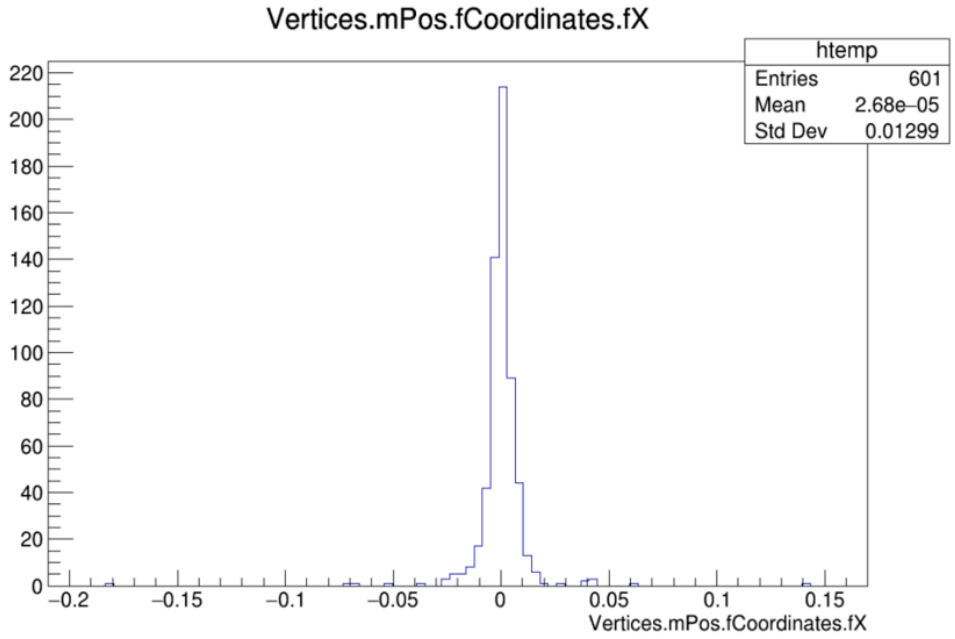

Figure 3.1: Primary vertices of particles in horizontal coordinate. There is a slight spreading of primary vertices beyond the the center of collision.

3.1 Expected Decay Muon Distribution in Global Muon Track

The number of decay muons from Kaon (K^+), pions, D mesons, and B mesons obtained from the Global Muon Track of pp collisions are shown in Table 3.2.

Table 3.2: Number of muon decay in GM Track of pp collisions

Decay [GeV]	μ number
$D \rightarrow \mu$	1945
$B \rightarrow \mu$	227
$\pi^+ \rightarrow \mu$	6842
$K^+ \rightarrow \mu$	3290
$K_0^L \rightarrow \mu$	72
$\tau^- \rightarrow \mu$	43
$\gamma \rightarrow \mu$	5

In this research, primary muons are defined to include muons decayed from non-hadrons (leptons, photons, W^+, W^-, W^0, Z^0, gluons, higgs, etc.) or any particles with PDG codes less than 54. From the O2 simulation, we obtained 48 primary muons produced from tau leptons and photons, with 43 and 5 each, respectively.

The peaks are mostly centered at DCA_T = 0.15 cm. However, the DCA_T distributions are not yielding clear different DCA_T patterns for each mother particle decaying into muons.

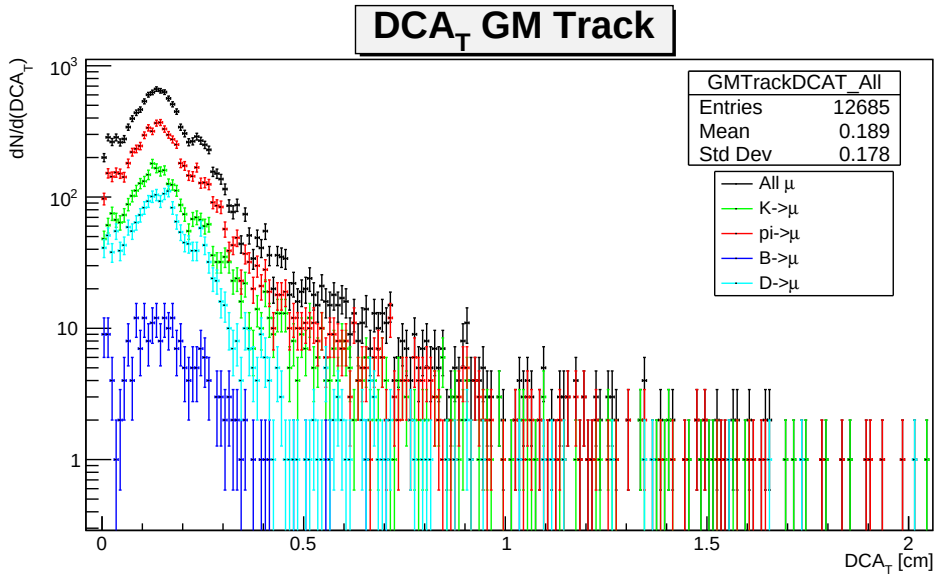

Figure 3.2: DCA_T distribution of muons for GM Track of pp.

Table 3.3: Number of muon decay in GM Track of Pb-Pb collisions

Decay [GeV]	μ number
$D \to \mu$	210
$B \to \mu$	13
$\pi^+ \to \mu$	1107
$K^+ \to \mu$	514
$K_0^L \to \mu$	0
$\tau^- \to \mu$	2
$\gamma \to \mu$	0

The number of decay muons from kaon (K^+), pions, D mesons, and B mesons obtained from the Global Muon Track of Pb-Pb collisions is shown in Table 3.3.

The statistics of muons obtained are fewer compared to pp, and it might not be sufficient for DCA_T histogram analysis. The formation of two peaks near DCA_T = 0.1 cm can be explained for a few reasons. When a meson decays into a muon, the resulting muon can have different lifetimes before it decays further. Some muons from meson decays have relatively short lifetimes and decay close to the primary vertex, resulting in a small DCA_T value. On the other hand, some muons have longer lifetimes and travel a significant distance from the primary vertex before decaying, leading to a larger DCA_T value.

We also calculate the DCA_T^2 distribution to investigate whether there are specific pattern distributions of muon decay points in certain ranges. In certain cases, the DCA_T^2 distribution of B and D meson decays may exhibit distinct features or show a specific pattern at certain DCA_T^2 ranges. This can be due to the underlying dynamics of the decays or the characteristics of the particles involved. From Figure

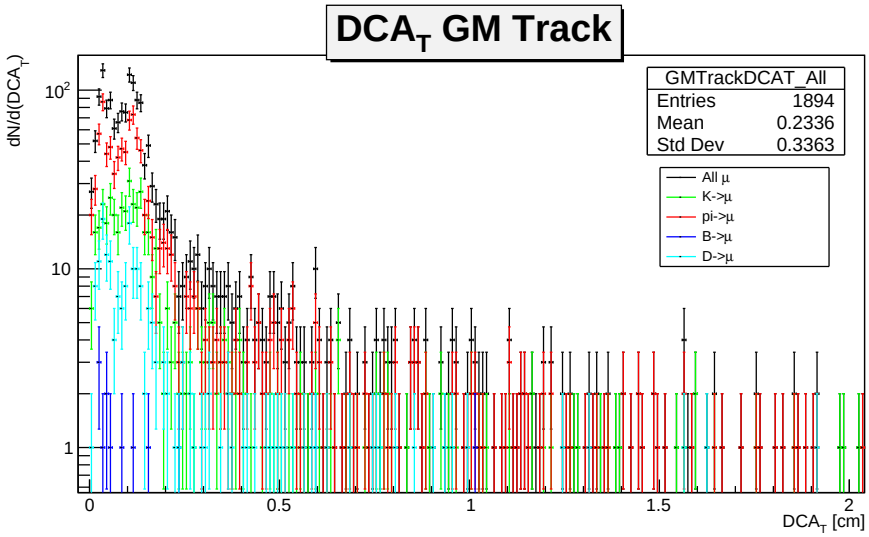

Figure 3.3: DCA_T distribution of muons for GM Track of Pb-Pb

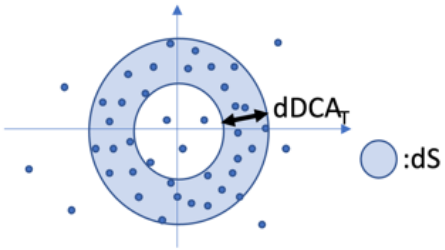

Figure 3.4: The formation of near uniform distribution in xy-plane at z=0 cm.

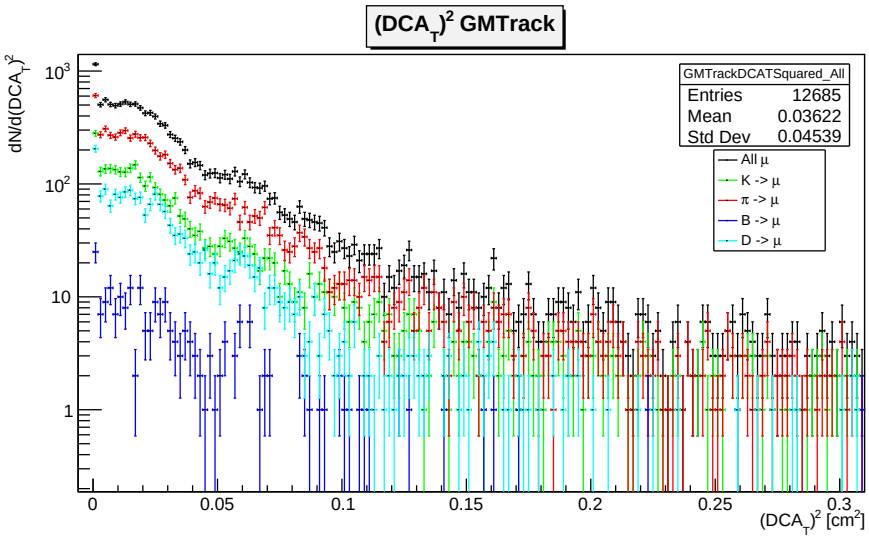

Figure 3.5: DCA_T^2 distribution of muons for GM Track of pp

3.5, we can see an almost uniform distribution below 0.02 cm^2 although that is not the case for Figure 3.6. Firstly, this can be attributed to the finite lifetimes of B and

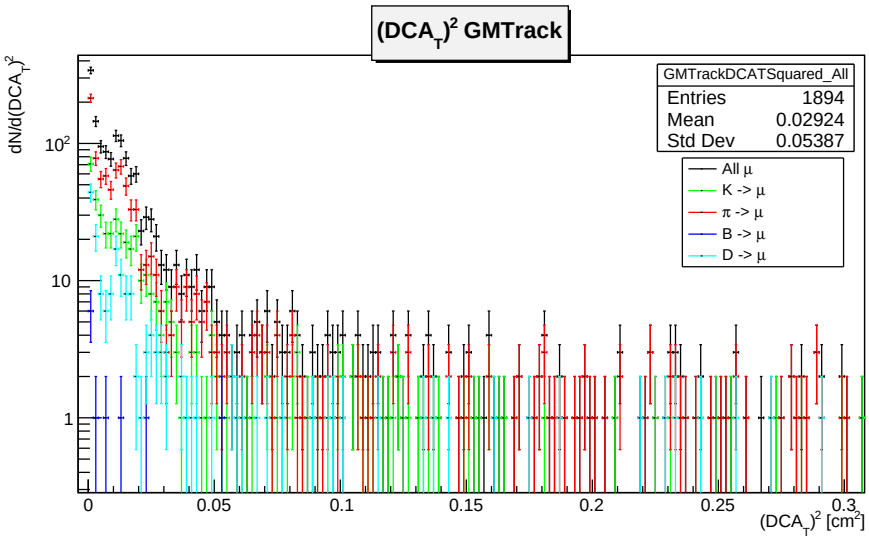

Figure 3.6: DCA$_T^2$ distribution of muons for GM Track of Pb-Pb

D mesons, as the muons originating from these decays would not have significant displacements from the primary vertex. Second, multiple scattering of muons as they traverse inside the material of the detector components can cause their trajectories to deviate, and they can no longer be reconstructed precisely to their decay points. The resolution of the detectors in the detector system may not be as good as the resolution in the tracker, leading to larger uncertainties in the DCA determination for global muon tracks. With no minimum bias setting applied in selection criteria, there will be a pile-up of additional muon tracks contributing to overall signals in the DCA_T distribution.

Ideally, we expect a uniform distribution of decay muons near $DCA_T^2 = 0$. If the decay muons have a wide range of momenta, it increases the chances of having small DCA_T^2 values. This is because particles with different momenta will have trajectories that are more likely to come close to each other, resulting in small DCA_T^2 values. Also, if decay muons are emitted isotropically in all directions, it can lead to a more uniform distribution of DCA_T^2 values. On the other hand, if there are specific angular correlations between the particles, such as back-to-back emission, it can result in a more structured DCA_T^2 distribution.

3.2 Expected Decay Muon Distribution in Monte Carlo Track

The number of decay muons from kaons, pions, D mesons, and B mesons obtained from Monte Carlo Track of pp collisions are shown in Table 3.4 and Table 3.5. From Figure 3.7 and 3.8, it is shown that muons from B and D mesons dominate at $DCA_T \leq 0.1$ cm with sharp peaks around DCA_T= 0 cm, while muons from kaons and pions dominate at $DCA_T \geq 0.1$ cm with lower distribution. The decay processes of B and D mesons typically involve longer lifetimes, allowing the decay muons to travel a certain distance before decaying. This can result in a broader distribution of DCA_T values, including a higher probability of observing muons with larger DCA_T values.

Table 3.4: Number of muon decay in MC Track pp collisions

Decay	μ number
D $\rightarrow \mu$	1919
B $\rightarrow \mu$	207
$\pi^+ \rightarrow \mu$	2230
$K^+ \rightarrow \mu$	1050
$K_0^L \rightarrow \mu$	27
$\tau^- \rightarrow \mu$	41
$\gamma \rightarrow \mu$	6

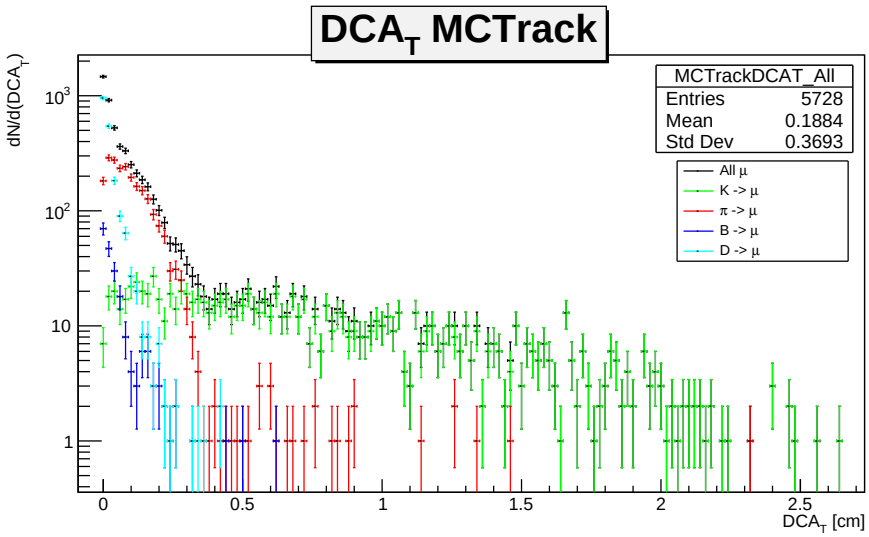

Figure 3.7: DCA$_T$ distribution of muons for MC Track pp

Figure 3.9 and 3.10 show the simulated distributions of decay muons for different p_T ranges. The DCA_T distributions of muons from D mesons and pions shows

Table 3.5: Number of muon decay in MC Track Pb-Pb collisions

Decay	μ number
D $\rightarrow \mu$	1193
B $\rightarrow \mu$	96
$\pi^+ \rightarrow \mu$	1418
$K^+ \rightarrow \mu$	681
$K_0^L \rightarrow \mu$	9
$\tau^- \rightarrow \mu$	17
$\gamma \rightarrow \mu$	0

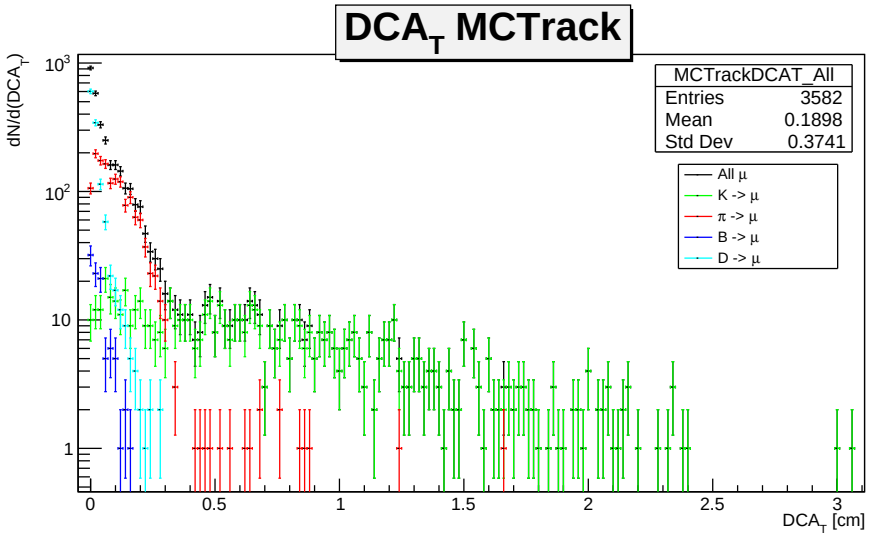

Figure 3.8: DCA_T distribution of muons for MC Track Pb-Pb

an increasing trend toward a sharp peak near DCA_T = 0 cm, while it remains considerably lower for B mesons and kaons. DCA_T distributions generally decrease with increasing p_T due to particle kinematics and multiple scatterings in the detector components. Higher p_T particles have larger momentum and experience less curvature in the magnetic field, resulting in smaller DCA_T. Multiple scattering causes random deviations in the particle trajectories and can contribute to larger DCA_T. However, higher p_T particles have larger momenta and are less affected by multiple scattering, resulting in smaller DCA_T. In case of B mesons, low count mainly the cause for lower distribution.

The DCA_T mean and resolution are extracted by a Gaussian functional as shown in Fig. 3.11 and Fig. 3.12. The DCA_T mean for all muons (signals and backgrounds) shows a decreasing trend, but it shows a somewhat decreasing trend for beauty (decay muons from B mesons). Generally, higher p_T particles tend to be produced with larger transverse displacements from the primary collision vertex. The presence of these secondary vertices can contribute to a larger average DCA_T for muons from charm compared to other particles. This might cause unclear trend

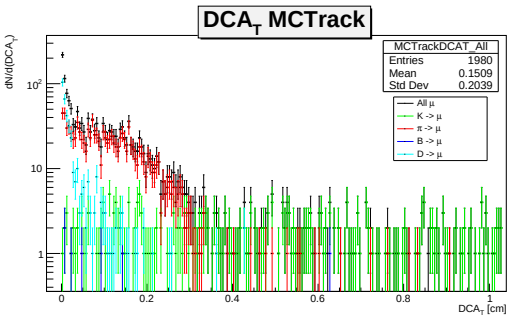

p_T: 0-0.5 GeV/c

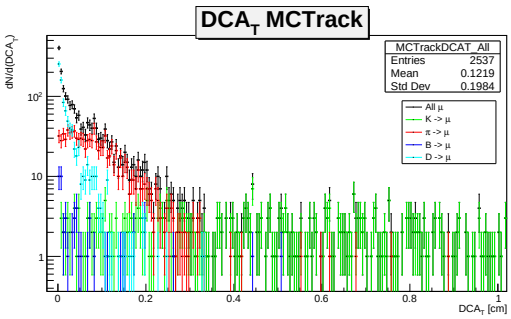

p_T: 0.5-1.0 GeV/c

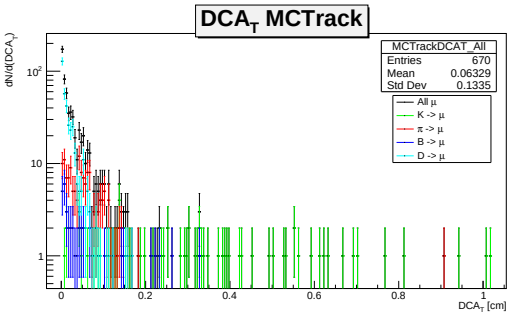

p_T: 1.0-1.5 GeV/c

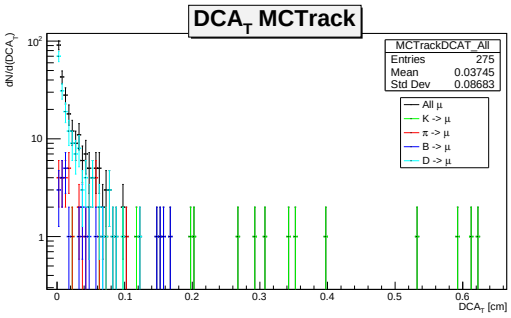

p_T: 1.5-2.0 GeV/c

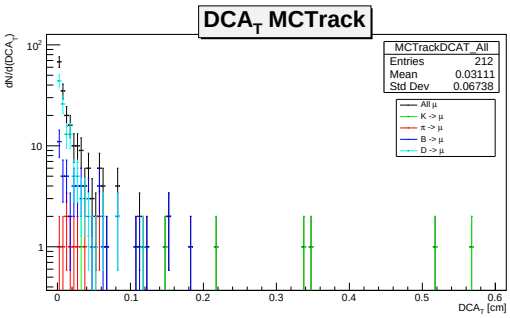

p_T: 2.0-4.0 GeV/c

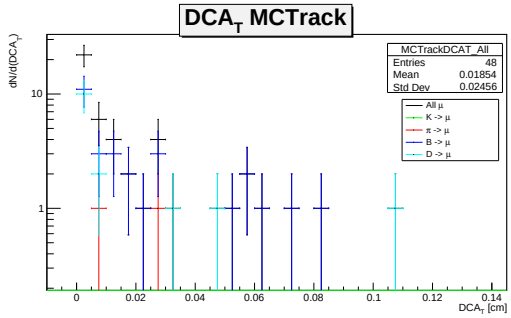

p_T: 4.0-7.0 GeV/c

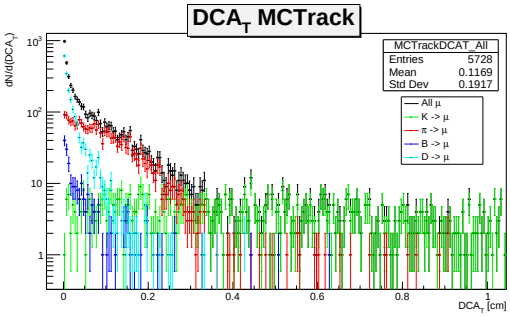

p_T: 0-10.0 GeV/c

Figure 3.9: DCA_T distributions of decay muons in different p_T ranges for MC track of pp.

for the charm. On the other hand, the DCA_T resolution trends show no particular dependence on particle types and generally decrease with increasing p_T as a bias of a tracking algorithm.

Table 3.6: Decay muons count in different p_T ranges for MC track of pp.

p_T [GeV]	Charm	Beauty	All μ
0-0.5	364	7	1980
0.5-1.0	872	55	2537
1.0-1.5	363	38	670
1.5-2.0	180	24	275
2.0-4.0	121	53	212
4.0-7.0	15	29	48
0-10.0	1919	207	5728

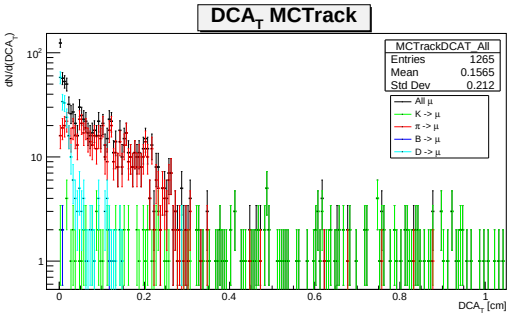

p_T: 0-0.5 GeV/c

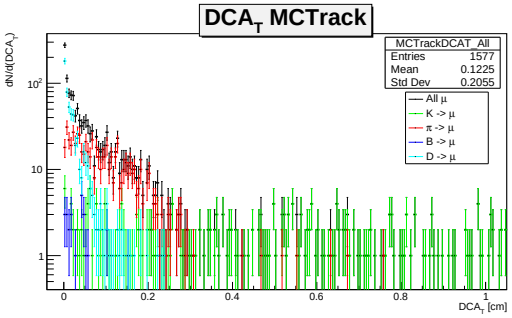

p_T: 0.5-1.0 GeV/c

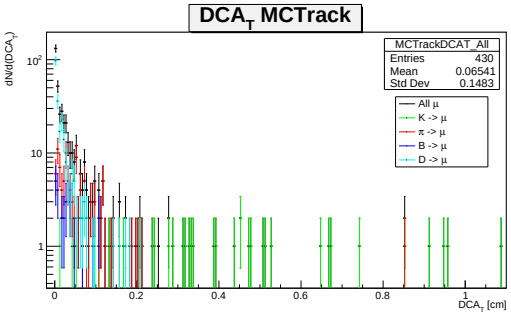

p_T: 1.0-1.5 GeV/c

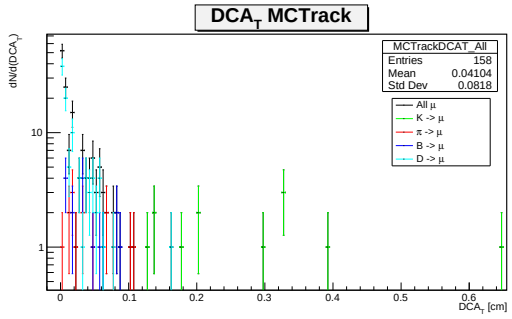

p_T: 1.5-2.0 GeV/c

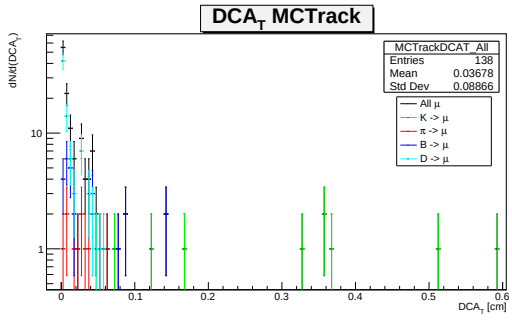

p_T: 2.0-4.0 GeV/c

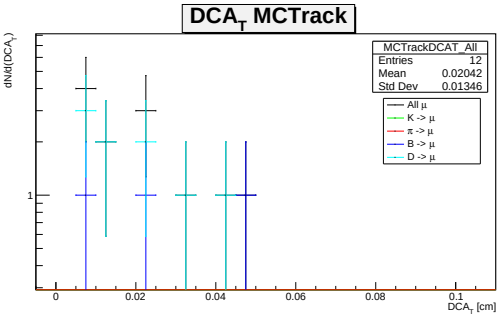

p_T: 4.0-7.0 GeV/c

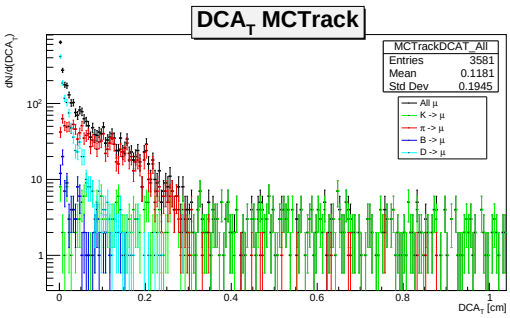

p_T: 0-10.0 GeV/c

Figure 3.10: DCA_T distributions of decay muons in different p_T ranges for MC track of Pb-Pb.

Table 3.7: Decay muons count in different p_T ranges for MC track of Pb-Pb.

p_T [GeV]	Charm	Beauty	All μ
0-0.5	228	3	1265
0.5-1	546	25	1577
1-1.5	231	24	430
1.5-2	98	16	158
2-4	80	25	138
4-7	9	3	12
0-10	1193	96	3581

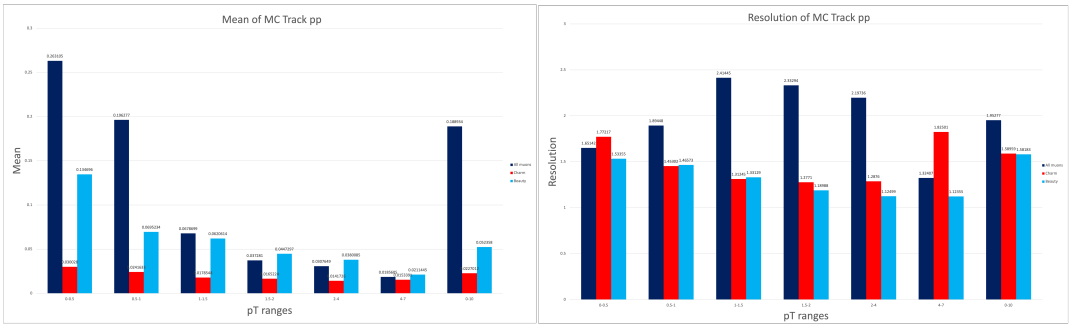

(a) (b)

Figure 3.11: (a) Mean and (b) resolution for MC track of pp.

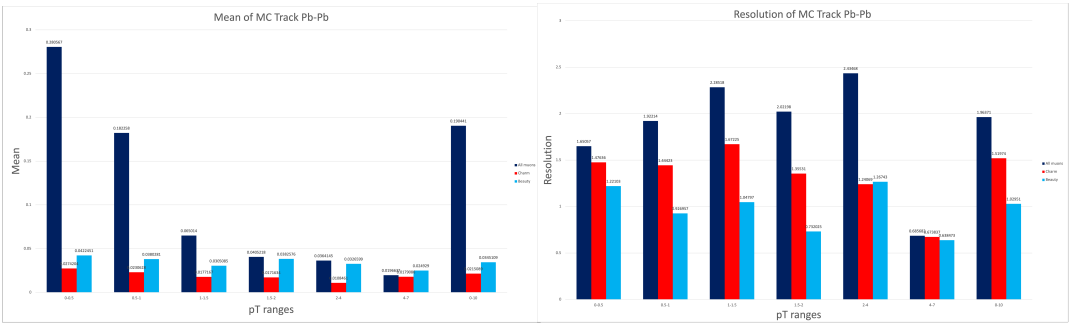

(a) (b)

Figure 3.12: (a) Mean and (b) resolution for MC track of Pb-Pb.

3.3 Signals and Background Muons in Monte Carlo Track

Fig. 3.13 and 3.14 show the simulated p_T distribution of signal muons (from charm and beauty) and background muons (from other sources) for pp and Pb-Pb collisions. Signal muons dominate background muons for the region $p_T \geq 1$ GeV/c because heavy flavor mesons like B and D mesons have larger masses and, therefore, their decay muons tend to carry higher momenta.

At $p_T \geq 1$ GeV, background muons dominate signal muons, caused by decays of lighter mesons, hadronic interactions, and low-energy processes. Fig 3.15 and 3.16 show the simulated DCA_T distribution of signal muons and background muons (top diagram), with the bottom diagrams showing the $\frac{\sqrt{S^3}}{B}$ cut-off distribution. The $\frac{S}{B}$ (signal-to-background) ratio is a useful metric for determining the cut-off condition in the shift of the generating point. However, when the cut-off is applied, the number of signal events decreases, leading to a loss of statistical significance. To address this issue, the $\frac{S}{B}$ ratio is weighted by $\sqrt{S}$, representing the statistical significance of the signal. This weighted ratio, known as $\frac{\sqrt{S^3}}{B}$, is used as an index. The highest point of the $\frac{\sqrt{S^3}}{B}$ distribution serves as a reference, considering the detection efficiency of the signal. This reference point, along with the efficiency, is examined to determine the optimal conditions for the final shift of the generating point. By incorporating both the statistical significance of the signal and the efficiency of detection, a comprehensive evaluation of the shift is performed to ensure reliable and accurate results.

From figures 3.15 and 3.16, it can be inferred that the count of signal muons rises above the background muons, reaching a maximum significant value near DCA_T = 0.03 cm. This indicates that the signal events are more significant compared to the background events near that specific point.

The peak occurring near zero suggests that the separation between the signal and background distributions is particularly noticeable at low values or close to the origin of the variable being analyzed. This region could correspond to a specific physical phenomenon or process of interest where the signal stands out prominently, making it easier to distinguish from the background. We use this information to decide on the suitable cut-off range to separate heavy flavor muons from the background: the DCA_T < 0.03 cm region is the most suitable.

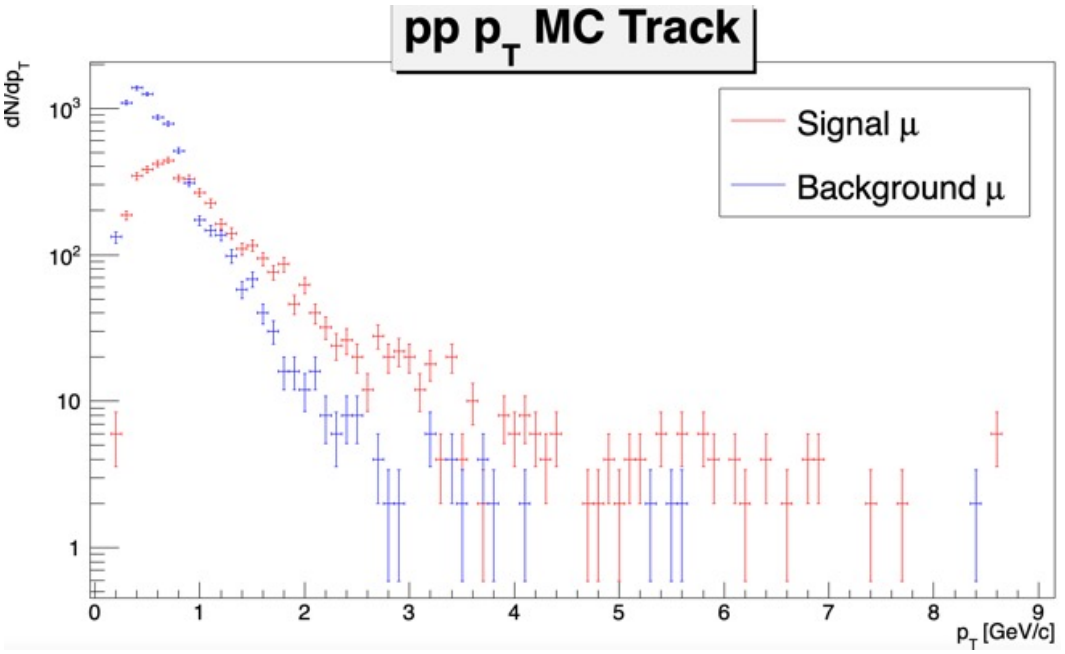

(a)

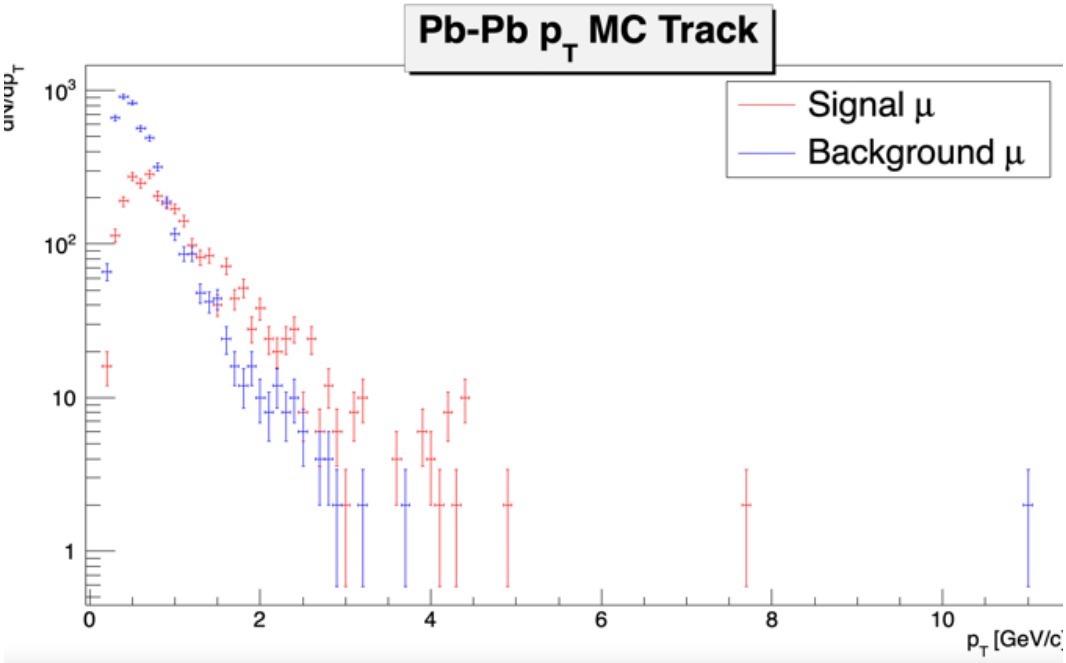

(b)

Figure 3.13: p_T distributions for signal muons and background muons for MC track of (a) pp and (b) Pb-Pb

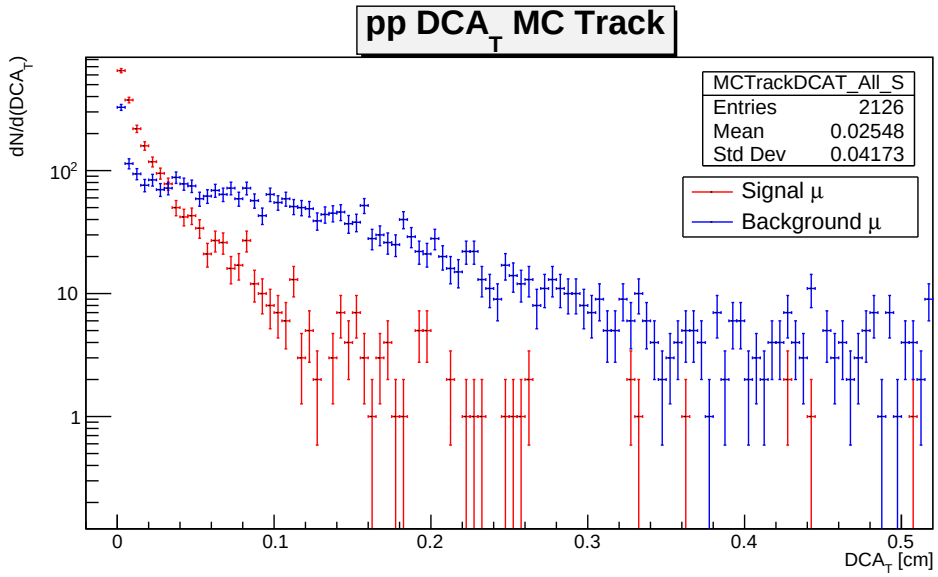

(a)

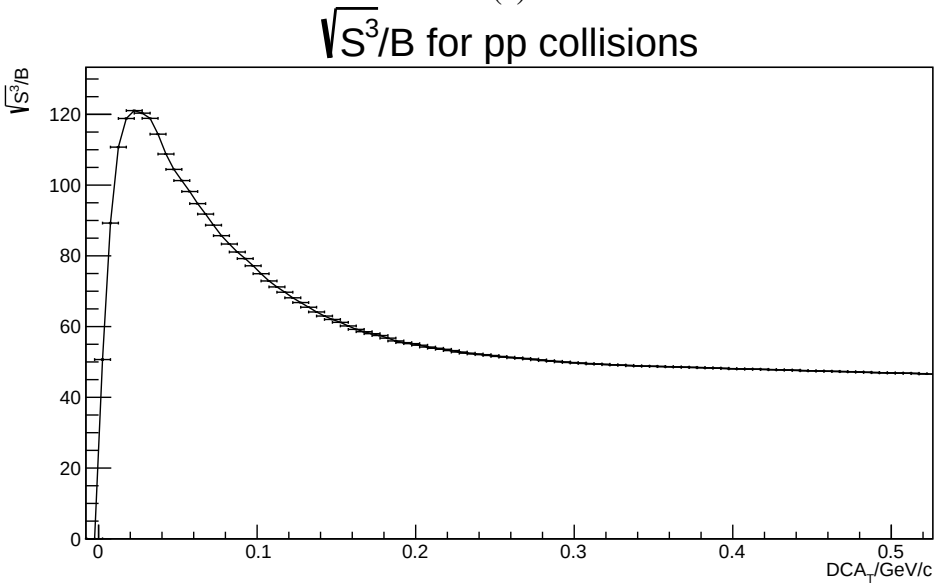

(b)

Figure 3.14: (a) DCA_T distributions for signal muons and background muons for MC track of pp and their (b) statistical significance, $\frac{\sqrt{S^3}}{B}$ distribution.

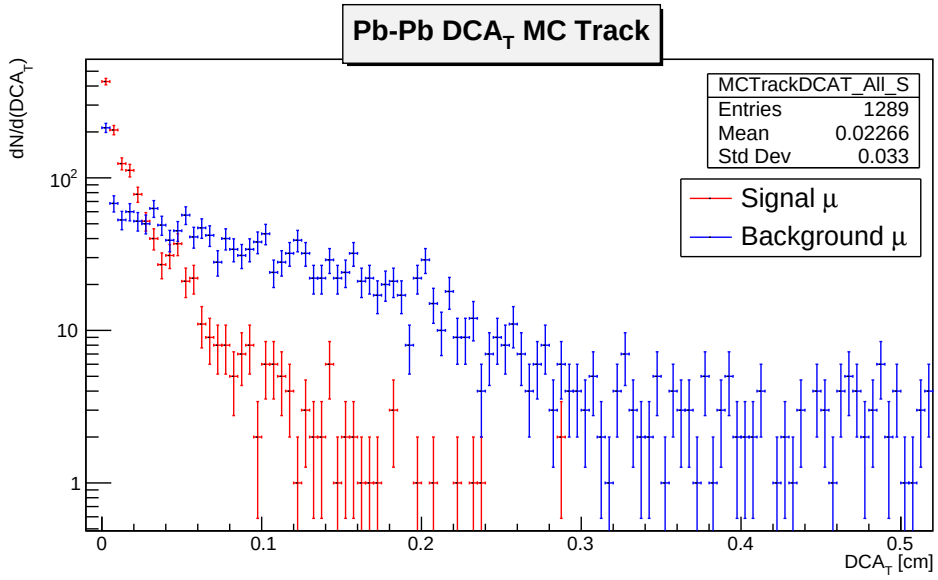

(a)

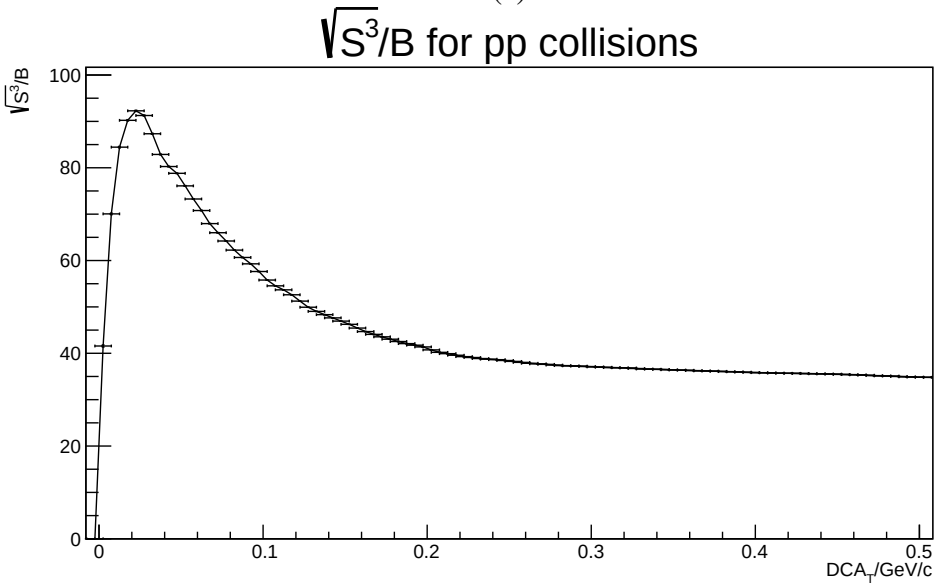

(b)

Figure 3.15: (a) DCA_T distributions for signal muons and background muons for MC track of Pb-Pb and their (b) statistical significance, $\frac{\sqrt{S^3}}{B}$ distribution

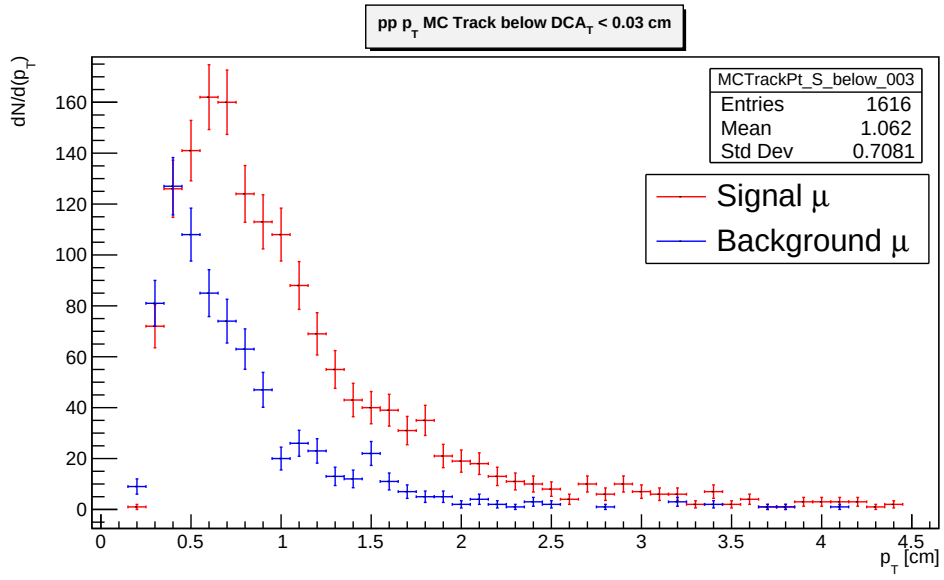

(a) p_T distributions for signal muons and background muons for MC track of pp after cut-off optimization (DCA_T < 0.03 cm). Background muons are significantly reduced and proportion of signals are maximized.

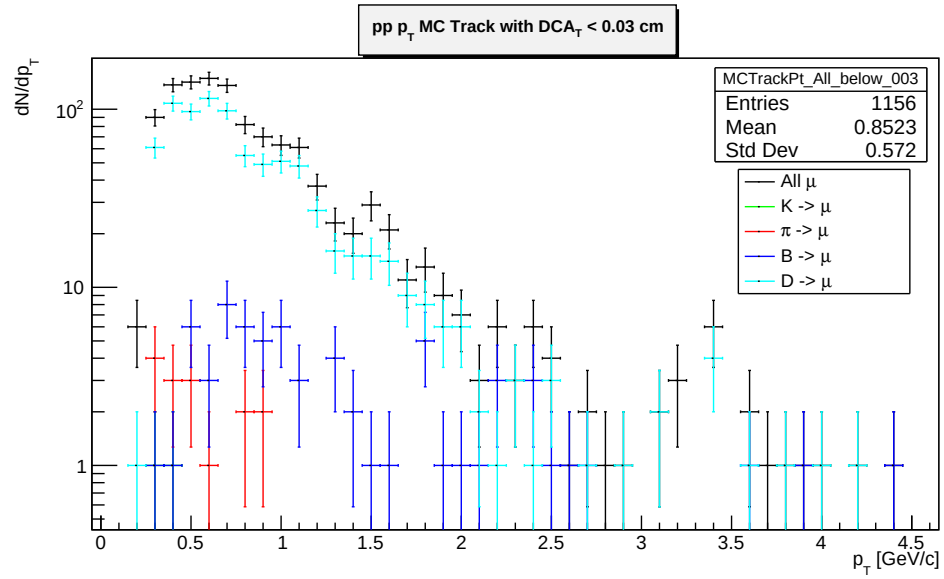

(a) p_T distributions for all muons for MC track of pp after cut-off optimization (DCA_T < 0.03 cm). Decay muons from K and π are significantly reduced, while proportion from B and D mesons are maximized.

Figure 3.16: p_T distributions result for pp after applying cutoff only for region DCA_T < 0.03 cm

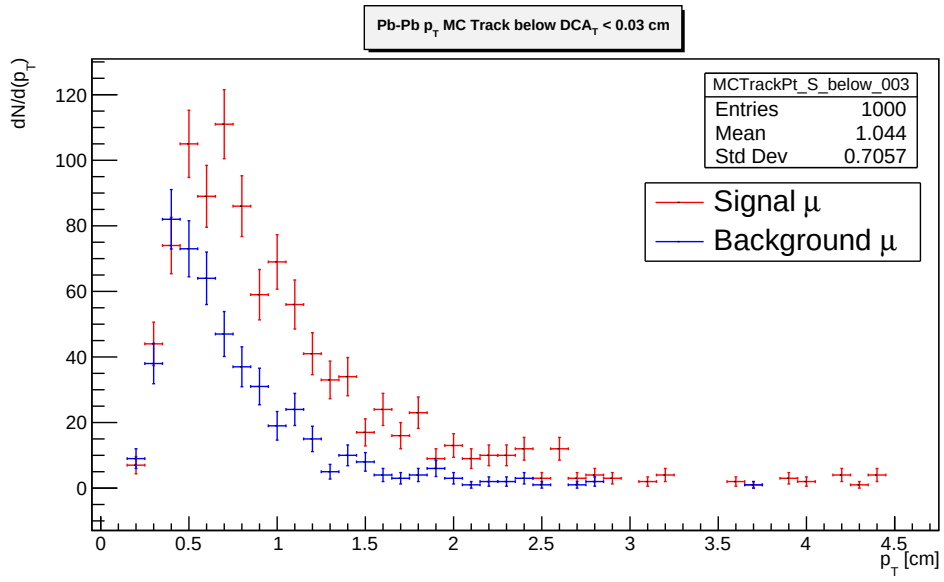

a) p_T distributions for signal muons and background muons for MC track of Pb-Pb after cut-off optimization (DCA_T < 0.03 cm). Background muons are significantly reduced and proportion of signals are maximized.

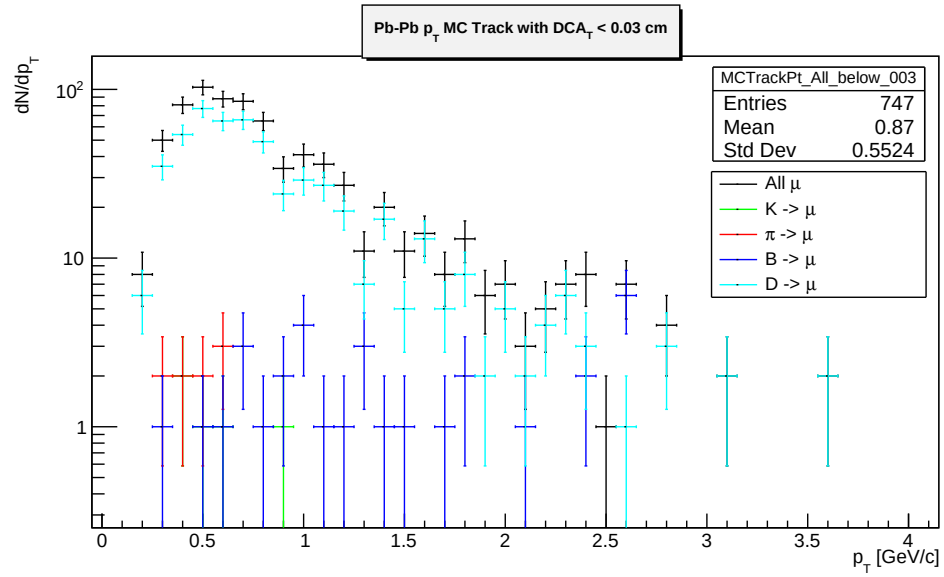

(a) p_T distributions for all muons for MC track of Pb-Pb after cut-off optimization (DCA_T < 0.03 cm). Decay muons from K and π are significantly reduced, while proportion from B and D mesons are maximized.

Figure 3.17: p_T distributions result for Pb-Pb after applying cutoff only for region DCA_T < 0.03 cm

3.4 Prompt decay muons from light mesons

Figure 3.18 and 3.19 show p_T and DCA_T distributions of light mesons (ρ, ω, η, and ϕ mesons). Prompt decay muons are muons that arise directly from the primary collision vertex in high-energy particle collisions. They are distinct from non-prompt muons, which originate from the decay of long-lived particles or secondary decay vertices.

The production of prompt decay muons from the primary vertex is intricately linked to the properties and interactions of the light mesons such as ρ, ω, η, and ϕ mesons. Their lifetimes are relatively short compared to heavy flavor mesons and are typically on the order of 10^{-23} to 10^{-24} s. This short lifetime is due to the decay processes associated with the weak interaction and the relatively small mass differences between the mesons' constituent quarks. These mesons are typically short-lived and decay rapidly, giving rise to prompt muons. The decay of heavy flavor mesons occurs via weak interactions, which are mediated by the exchange of W and Z bosons.

Another characteristic of prompt decay muons is their straighter trajectory compared to other charged particles. This is due to the fact that muons are not strongly affected by electromagnetic interactions within the detector material, unlike charged hadrons such as pions or kaons. Muons, being leptons, only interact weakly with the detector material and experience minimal energy loss through ionization or radiation. As a result, prompt muons tend to exhibit minimal scattering and follow relatively straight paths from the primary vertex to the muon detectors.

Table 3.8: Parent particles and their decay muon count in pp.

Meson Types	μ Count
η	76
ω	63
ρ	32
ϕ	6
Total	177

Table 3.9: Parent particles and their decay muon count in Pb-Pb.

Meson Types	μ Count
η	42
ω	60
ρ	17
ϕ	8
Total	127

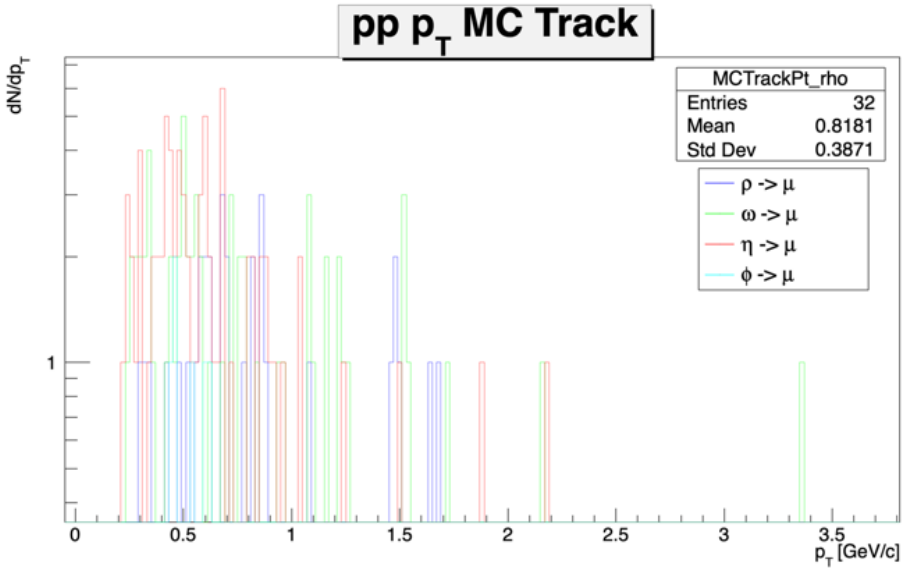

(a)

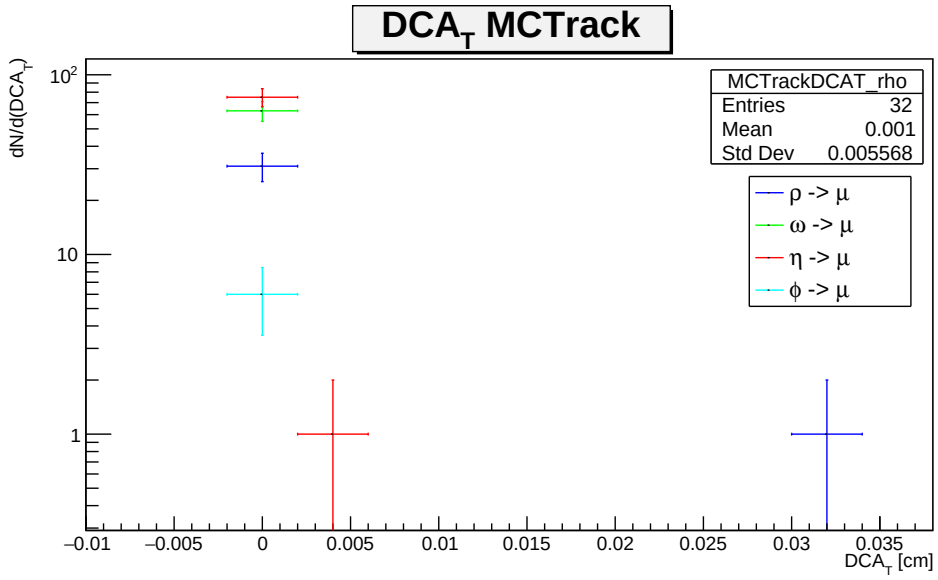

(b)

Figure 3.18: (a) p_T and (b) DCA_T distributions of prompt decay muons from light mesons for MC track of pp.

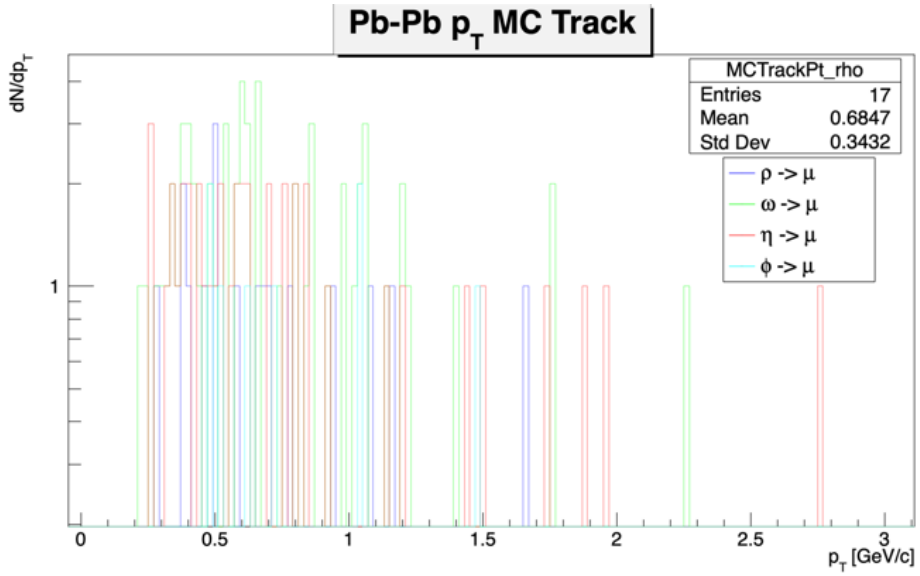

(a)

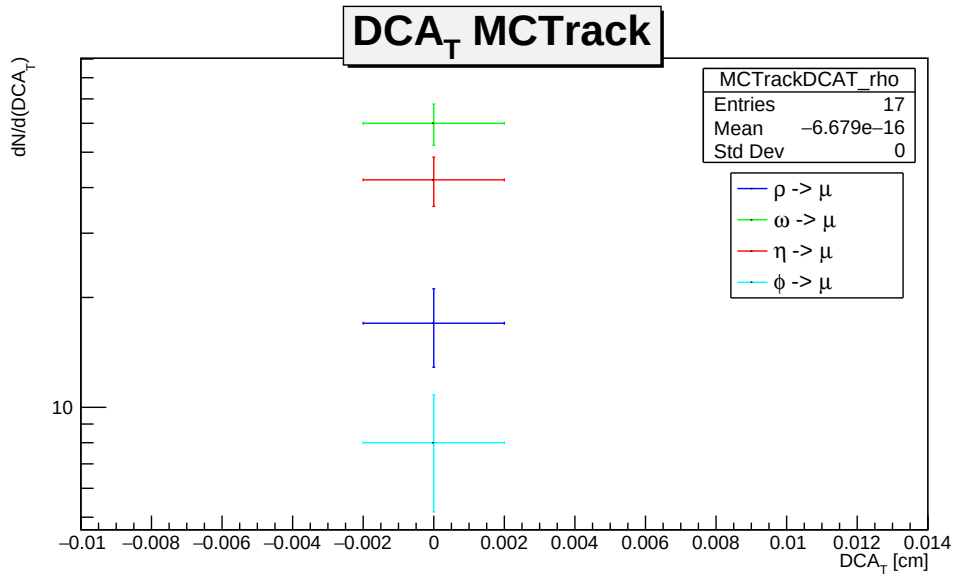

(b)

Figure 3.19: (a) p_T and (b) DCA_T distributions of prompt decay muons from light mesons for MC track of Pb-Pb.

Chapter 4

Summary

This paper focuses on the study of charm and beauty mesons' decay muons in the ALICE detector at CERN. The analysis strategy involves using the offset and distance of closest approach (DCA) quantities, along with other kinematic parameters, to estimate the decay length of B and D mesons, which is related to their lifetime.

The study primarily relies on simulations to investigate various aspects. The primary analysis technique for measuring charm and beauty yields in the single muon channel is based on fitting the DCA_T distribution. Proper DCA_T results were obtained from a simulated kinematic MC file, proving its reliability compared to MFT and GM files for DCA_T calculations. The MC track simulation has shown better DCA_T distribution results for B and D mesons compared to GM track simulation, suggesting the influence of multiple scattering in ALICE detector components affecting accuracy of the track matching.

At $DCA_T > 0.1$ cm, muons from pion and kaon decays dominate the DCA_T distribution with mostly wider distribution, while at $p_T > 1$ GeV/c, muons from charm-hadron and beauty-hadrons decays dominate for small DCA_T values ($DCA_T < 0.1$ cm). Cutoff optimization with p_T and DCA_T information were conducted, and signal yield and background calculations are obtained. The analysis has shown a high statistical significance of signal muons compared to background muons near $DCA_T < 0.03$ cm so we have decided that would be a good separation point. To separate muons from pions and kaons below $DCA_T < 0.03$ cm and maximize signals (from B and D mesons) while filtering background (from other muons), rejection techniques are implemented. As a result, B mesons and D mesons decay muons have been well separated from pions and kaons in the low transverse momentum region ($p_T \leq 4$ GeV/c). Additionally, prompt muons from light mesons (ρ, ϕ, η, and ω mesons) are concentrated at $DCA_T = 0$ cm.

However, the low count of B mesons prevents meaningful analysis, while the high count of charm mesons requires rejection of minimum bias from charmonium for better accuracy. The true matching also needs to be calculated to see how false

matching tracks can impact the efficiency of the overall measurement.

In the actual experiment, Muon Forward Tracker (MFT) plays a crucial role in the study of charm and beauty mesons' decay muons by providing vertexing capabilities at forward rapidity. It effectively separates muons from charm-hadron and beauty-hadron decays from the light-flavor background, with respective p_T cutoffs of about 0.5 GeV/c and 2 GeV/c. Notably, the longer lifetime of beauty hadrons results in muons from beauty-hadron decays having a larger average separation from the primary vertex compared to those from charmed hadrons.

Promising performance studies have demonstrated successful separation of muons from charm and beauty decays at forward rapidity using real data from LHC Run 3. The ongoing analysis involves pp collisions at 13.6 TeV collected in 2022, and data taking for Pb-Pb collisions at 5.36 TeV is expected in October 2023.

Bibliography

[1] Povh, R., Rith, K., Scholz, C., and Zetsche, F. *Particles and Nuclei: An Introduction to the Physical Concepts*. Springer, 2015.

[2] The CMS Collaboration. *CMS Physics Technical Design Report: Addendum on High Density QCD with Heavy Ions*, volume 34. Journal of Physics G, Oct 2007. URL https://iopscience.iop.org/article/10.1088/0954-3899/34/11/008.

[3] Fayyazuddin Riazuddin. *A Modern Introduction to Particle Physics*. World Scientific, 2011.

[4] P. A. Zyla and et al. (Particle Data Group), editor. *Review of Particle Physics*. Particle Data Group, 2020. Available online at http://pdg.lbl.gov/2020/reviews/rpp2020-rev-passage-particles-matter.pdf.

[5] Tauro, Arturo. *ALICE Schematics*. Number ALICE-PHO-SKE-2017-001 in ALICE Photos / ALICE / ALICE Sketches. CERN, 2017. URL https://cds.cern.ch/record/2263642. General Photo.

[6] Christian Finck for ALICE Muon Spectrometer Collaboration. *The Muon Spectrometer of the ALICE*, volume 50. Institute of Physics Publishing, 2006. doi: 10.1088/1742-6596/50/1/056. Proceedings of the 5th International Conference on Physics and Astrophysics of Quark Gluon Plasma.

[7] ALICE-O2 Collaboration. *ALICE O² Project*. 2018. URL https://alice-o2-project.web.cern.ch/alice-o2-project. Submitted by gpachoud on May 16, 2018, Accessed on July 24, 2023.

[8] Kazuya Nagashima. *Energy Loss of Charm and Bottom Quarks in Quark-Gluon Plasma Created in Au+Au Collisions at* $\sqrt{s_{\mathrm{NN}}} = 200$ *GeV*. 2019.

[9] F. J., Ynduráin. *Quantum Chromodynamics: An Introduction to the Theory of Quarks and Gluons*. Springer, 2006.

[10] Pasechnik, Roman and Šumbera, Michal. *Phenomenological Review on Quark–Gluon Plasma: Concepts vs. Observations*. 2017. URL https://arxiv.org/abs/1611.01533v3. arXiv:1611.01533v3 [hep-ph].

[11] CERN. *Heavy Ions and Quark-Gluon Plasma*. URL https://home.cern/science/physics/heavy-ions-and-quark\

-gluon-plasma. Accessed on 2023-07-24.

[12] M. G. Mustafa and M. H. Thoma. *Energy Loss of Heavy Quarks in the Quark-Gluon Plasma*. Elsevier, 1998. doi: 10.1016/S0370-2693(98)00452-2. Physics Letters B, Volume 428, Issues 3–4, Pages 234-238.

[13] T. Matsui and H. Satz. *J/ Suppression by Quark-Gluon Plasma Formation*. Elsevier, 1986. doi: 10.1016/0370-2693(86)91404-8. Physics Letters B, Volume 178, Issues 4, Pages 416-422.

[14] S. Chatrchyan and et al. (CMS Collaboration). *Observation of Sequential Suppression in PbPb Collisions*. American Physical Society, 2012. doi: 10.1103/PhysRevLett.109.222301. Physical Review Letters, Volume 109, Issue 22.

[15] S. Cao and et al. *Determination of Heavy-Quark Fragmentation Functions and their Uncertainties*. Springer, 2016. doi: 10.1007/JHEP01(2016)006. Journal of High Energy Physics, Volume 2016, Issue 1.

[16] N. Brambilla and et al. (Quarkonium Working Group). *Heavy Quarkonium: Progress, Puzzles, and Opportunities*. Springer, 2011. doi: 10.1140/epjc/s10052-010-1534-9. The European Physical Journal C, Volume 71, Issue 4.

[17] The ALICE Collaboration. *Upgrade of the ALICE Experiment: Addendum to the Letter of Intent*. CERN, 2013. URL https://cds.cern.ch/record/1582252. ALICE-UG-003 CERN-LHCC-2013-014 / LHCC-I-022-ADD-1.

[18] S. Agostinelli and et al. *Geant4 - A Simulation Toolkit*, volume 506 of *Nuclear Instruments and Methods in Physics Research A*. Elsevier, 2003. doi: 10.1016/S0168-9002(03)01368-8.

[19] Christian Bierlich, Smita Chakraborty, Nishita Desai, Leif Gellersen, Ilkka Helenius, Philip Ilten, Leif Lönnblad, Stephen Mrenna, Stefan Prestel, Christian T. Preuss, Torbjörn Sjöstrand, Peter Skands, Marius Utheim, and Rob Verheyen. *A comprehensive guide to the physics and usage of PYTHIA 8.3*. 2022. URL https://pythia.org/documentation/. LU-TP 22-16, MCNET-22-04.

[20] Ren Ejima. *Development of Muon Reconstruction Method Based on Machine Learning for ALICE Run 3 and Improvement of Performance for Verification of Origin of Hadronic Mass*. 2023.

[21] The ALICE Collaboration. *Technical Design Report for the Upgrade of the Online–Offline Computing System*. 2015. ALICE-TDR-19, CERN-LHCC-2015-006, June 2, 2015.

Acknowledgement

First of all, I would like to express my gratitude to everyone who was involved in my research. I would like to thank Professor Kenta Shigaki for his efforts in guiding me through useful discussions and advice for the research. I have been given many opportunities to participate in advanced scientific research, workshops, and conferences. In particular, my scientific presentations have been very beneficial learning experiences. I would also like to thank Associate Professor Yorito Yamaguchi and Assistant Professor Satoshi Yano for their constructive comments and guidance. You have been helping me a lot through the simulations and analysis framework, despite the time constraint. I am eager to delve further into this area, given the opportunity. I extend my thanks to Professor Kensuke Homma, mainly for the interesting laboratory lessons and insightful comments in the meetings. Associate Professor Takahiro Miyoshi also provided assistance during the courses, although I don't usually get the chance to talk with you. Researcher Masanori Ogino also helped me with managing the computer programming. I would also like to thank all the other Japanese students who have given me a lot of help, including physics discussions and support with my research work. Without their support, I would have been lost. Thank you, everyone, for giving me great memories while I am in Japan.

Thank you also to JICA for their sponsorship and other support they have provided me. I would like to express my gratitude to my family for their moral and spiritual support. Finally, I offer my thanks to God for granting me the chance to spend my time gaining knowledge in Japan, despite the fleeting nature of life.